Antitumour Activity of a Hinge- and Fc-engineered Chimeric Heavy-chain Antibody.

By: Calvin D'Eall
Supervisor: Jamshid Tanha

A Thesis submitted to The
School of Graduate Studies
University of Ottawa

In partial fulfillment of the requirements for the degree
of
Master's of Science
Department of Microbiology and Immunology
Faculty of Medicine

Table of Contents

5. Discussion

Abstract

EG2-hFc is an ≈ 80 kDa chimeric heavy-chain antibody comprised of human IgG1 hinge and fragment crystallisable bivalently linked to EG2; a camelid-derived, heavy chain antibody variable domain specific for the human epithelial growth factor receptor 1 and its associated EGFRvIII mutant. Though previous work revealed EG2-hFc to demonstrate impressive *in-vivo* tumour accumulation, it's therapeutic potential, as well as that of chimeric heavy-chain antibodies in general, remains largely unexplored. With this in mind, our current study was successful in showing that EG2-hFc could facilitate *in-vitro* antibody-dependent cell-mediated cytotoxicity of epithelial growth factor receptor-positive breast cancer cells. Additionally, EG2-hFc's intrinsic cytotoxicity was augmented following the implementation of engineering strategies that are currently being explored in the context of conventional anti-cancer monoclonal antibodies: including the modification of a conserved *N*-linked C_H2 glycan, as well as the alteration of EG2-hFc's hinge length. Collectively, these findings contribute to the growing body of research that has revealed chimeric heavy-chain antibodies to be a promising class of novel anti-tumour therapeutics.

List of Abbreviations

^{51}Cr	Sodium-chromate
a.a.	Amino acid
Ab	Antibody
ABD	Antigen binding domain
ADCC	Antibody-dependent cell-mediated cytotoxicity
AF405	Alexa-fluor 405
Asn297	Asparagine 297
B_{max}	Binding-maximum
CBSWB#	Canadian blood services whole-blood sample #
CD16a	Fc gamma receptor IIIa
CD	Circular dichroism
cDNA	Complementary deoxyribonucleic acid
CDC	Complement-dependent cytotoxicity
CDR	Complementarity-determining region
C_H1	Constant heavy-chain 1
C_H2	Constant heavy-chain 2
C_H3	Constant heavy-chain 3
cHCAb	Chimeric Heavy-chain antibody
CHO	Chinese hamster ovary cell
C_L	Constant light-chain
CRA	^{51}Cr release assay
DSB	Disulfide Bond
DTT	Dithiothreitol
E_C50	Half-maximal effective concentration
EGF	Epidermal growth factor
EGFR	Epidermal growth factor receptor
E:T	Effector to target ratio
Fab	Fragment antigen-binding
FBS	Fetal bovine serum
Fc	Fragment crystallizable
FcR	Fragment crystallizable receptor
FcRn	Neonatal Fc receptor
FDA	Federal drug administration
FF	Fraction folded
FITC	Fluorescein isothiocyanate
FUT8	Fucosyltransferase 8
GlcNAc	*N*-acetyl-glucosamine
GMD	GDP-mannose 6-dehydrogenase
GnT-III	1.4-*N*-acetylglucosaminyltransferase III
HCAb	Heavy-chain antibody
HEK	Human embryonic kidney cell
Her2	Epidermal growth factor receptor 2
hFc	Human hinge-fragment crystallizable

IFN-γ	Interferon gamma
IgG1	Immunoglobulin G 1
IL-2	Interleukin 2
IL-2R	Interleukin 2 receptor
K_D	Dissociation constant
LAK	Lymphokine-activated killer cells
LBD	Ligand binding domain
lh-HCAb	Long-hinge heavy-chain antibody
mAb	Monoclonal antibody
MBL	Mannose-binding lectins
MFI	Mean fluorescence intensity
MOA	Mechanism of action
NK	Natural killer cell
NR	Non-reducing
PBMC	Peripheral blood mononuclear cell
PBS	Phosphate-buffered saline
PE	Phycoerythrin
R	Reducing
RMD	GDP-6-deoxy-D-lyxo-4-hexulose reductase
RT	Room temperature
SB	Staining buffer
ScFv	Single-chain variable fragment
SDS-PAGE	Sodium dodecyl sulfate-polyacrylamide gel electrophoresis
SEC	Size-exclusion chromatography
SNP	Single nucleotide polymorphism
SPR	Surface plasmon resonance
TAA	Tumour-associated antigen
TGFα	Transforming growth factor alpha
T_m	Thermal-unfolding midpoint
V_H	Human variable heavy chain
V_HH	Camelid variable heavy chain
V_L	Variable light chain
wt	Wild-type

List of Figures

1. Introduction

1.1 Monoclonal antibodies as anti-tumour therapeutics:

At the start of the 20th century Paul Ehrlich envisioned the existence of therapeutic "magic bullets", which he believed would revolutionize the emerging field of molecular medicine (1). Remarkably, nearly three-quarters of a century later, Hohler and Milstein successfully produced what many hoped would be the manifestation of Ehrlich's anticipated molecules: hybridoma-derived monoclonal antibodies (mAbs) (2). Disappointment soon followed, as seminal research revealed these murine derived mAbs to be rife with features that would ultimately stifle their therapeutic application. This included their propensity to trigger the immunogenic development of human anti-mouse antibodies in treated patients, as well as their failure to engage with beneficial features of the human immune response: restrictions arising from their murine lineage (3). Despite these initial constraints, the technological advances being made in molecular biology provided hope that the suspected potential of mAbs would inevitably be realized. Nearly two decades after Hohler and Milstein's seminal research, these suspicions were confirmed following the development of recombinant DNA technology, which brought with it the chimeric and humanized mAb: propelling the field of antibody engineering to the scientific forefront (2, 4).

The now pervasive chimeric and humanized mAbs, possessing either murine variable domains or complementarity-determining regions (CDRs) linked to human constant domains, respectively, proved capable of overcoming the limitations faced by their purely murine predecessors (1). Since their initial inception, this formerly novel class of therapeutics has gone on to achieve unprecedented levels of success, with more than 30

mAbs currently approved for clinical use, with nearly countless others presently undergoing clinical and pre-clinical evaluations: making mAbs both the fastest growing and largest class of therapeutics (5). However, this success has been underrepresented in the context of solid-tumour immunotherapies, as only 7 of the 16 FDA approved anti-cancer mAbs are currently used in their treatment; though solid-tumours account for greater than 85% of all reported cancers (1, 6). This disproportionality is partially attributable to the notoriously tough microenvironment and vasculature of solid tumours compared to haematological cancers: characterized by increases in both blood viscosity and interstitial fluid pressure (1). Importantly, these features have been shown to directly prevent efficient tumour penetration and accumulation as a result of mAb mass (≈ 150 kDa) (Fig. 1a), since the speed of tumour diffusion is inversely proportional to an objects molecular mass (1, 7). Another limitation common amongst the current repertoire of FDA approved solid-tumour mAbs is their primary inhibitory function, which acts by neutralizing the oncogenic signal emanating from each mAbs respective antigenic target (8). Though mAbs employing this inhibitory mechanism-of-action (MOA) have had success as components of various combined therapies, they typically provide only a transient slowing of tumourigenesis when applied individually; a recurring feature likely attributable to the now outdated and myopic view that neutralizing a single oncogenic signal will effectively halt and reverse oncogenesis (9-12). Instead, current research suggests that the complex network of signals, receptors, and mutations that drive tumour progression likely demand a more nuanced intervention (12). In response to these limitations, researchers have begun exploring alternatives to conventional mAbs that possess characteristics better suited to the treatment of various indications, including solid-tumours. Such efforts have focused on the

use of modular antigen-binders, such as single-chain variable-fragments (scFvs) (Fig. 1b-d) and humanized single-domain antibodies (sdAbs) (Fig. 1e-g), which can be used to assemble remarkably compact antigen binding constructs: overcoming the tumour accumulation limitations faced by conventional mAbs (1). Furthermore, such novel constructs may be further engineered to halt tumourigenesis by mechanisms other than the inhibition of a single oncogenic signal. For instance, constructs possessing multiple antigenic specificities have been shown to effectively halt tumourigenesis by neutralizing multiple oncogenic signals (13, 14). Alternatively, current research has revealed antibody-dependent cell-mediated cytotoxicity (ADCC) as an under-utilized and promising alternative to oncogenic inhibition (15-16). Collectively, the ability to engineer constructs exhibiting such features has spurred the development of a new generation of anti-tumour therapeutics, with the potential to overcome the limitations faced by the current generation anti-cancer mAbs.

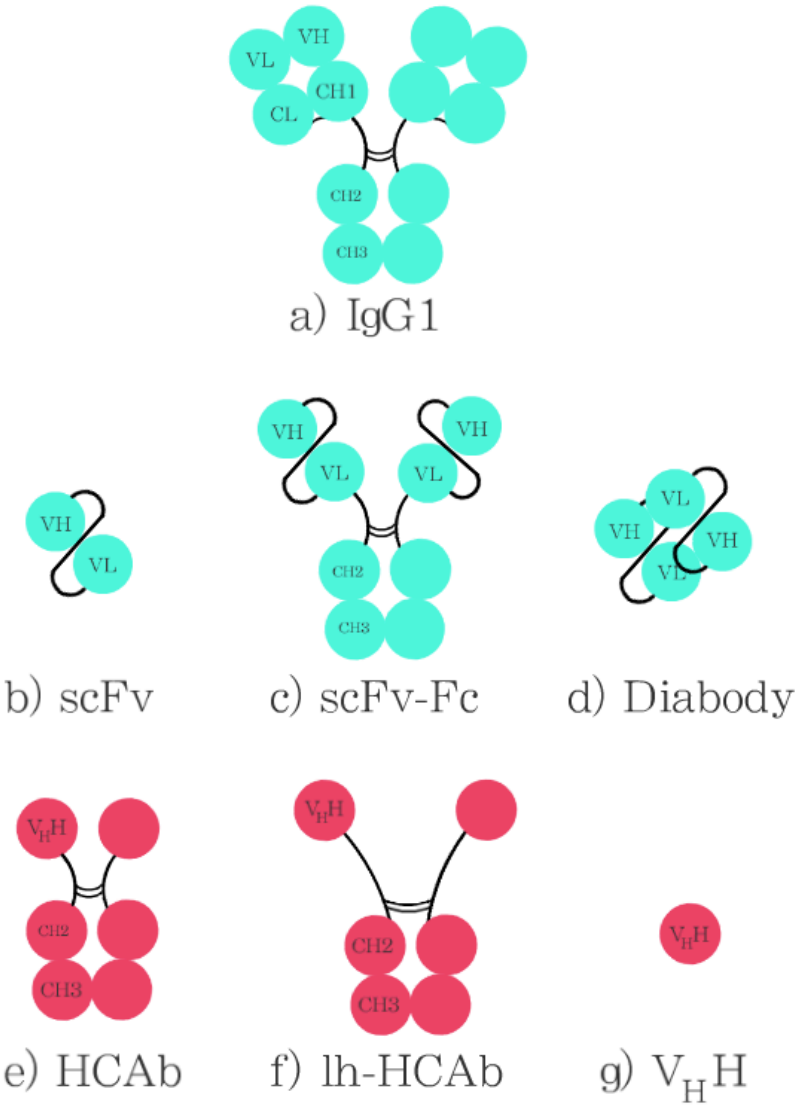

Figure 1: Conventional versus novel antibodies and antibody-based constructs
a) ≈ 150 kDa IgG1 is the most abundant IgG in human serum, with two inter-chain DSBs located in the lower hinge region, while the upper-hinge DSB connects the heavy and light chains of the Fab. **b-d)** ScFvs are comprised of linked V_H and V_L chains, which may be bivalently attached to hFc or linked together to give diabodies: with sizes of ≈ 25 kDa, ≈ 106 kDa and ≈ 50 kDa, respectively. **e)** The hinge length of a typical HCAbs (size ≈ 80 kDa) is comparable to that of IgG1, but the missing Fab chains give rise to a uniquely short distance between the V_HH (≈ 80 Å). **f)** Long-hinge camelid HCAb (size ≈ 90 kDa) contains an extended hinge, with a distance between V_HH (≈ 140 Å) similar to the distance between CDRs of cIgG1 (≈ 160 Å). **g)** Lastly, monomeric V_HH (≈ 13 kDa) can be expressed independently from the hFc of HCAb, giving one of the smallest antigen-binding structures presently known. V_HH may be linked to human IgG hinge-Fc, as well as humanized to reduce their potential immunogenicity.

1.2 Antibody dependent cell-mediated cytotoxicity and the CD16a polymorphism

The aforementioned limitations faced by inhibitory mAbs have prompted researchers to look toward alternative methods of halting tumourigenesis: a paradigm-shift exemplified by the evolving therapeutic interest in the FDA approved, neutralizing mAb: cetuximab. Following its initial clinical use, a sizeable portion of treated patients acquired resistance to cetuximab's primary and intended inhibitory MOA (11, 17-18). The onset of this resistance was found to coincide with the emergence of the EGFRvIII: a mutated variant of cetuximab's antigenic target, the epidermal growth factor receptor-1 (EGFR) (17). The EGFRvIII was shown to be constitutively active in the absence of receptor ligand, and thus unresponsive to cetuximab's neutralizing MOA (19-20). Consequently, interest in cetuximab's intended inhibitory function waned; only to be supplanted with a recently described ability to facilitate an alternative means of solid-tumour cell killing via antibody-dependent cell-mediated cytotoxicity (ADCC) (15-16, 21-22). An integral component of the adaptive immune response, ADCC is defined by the interaction between three central components: 1) a target (such as a cancer cell), lysed by 2) an effector cell, as mediated by 3) an antibody (Fig. 2) (23). Though facilitated by a variety of effector cell types, including macrophages and eosinphils, classical ADCC is carried out by the aptly named natural killer cell (NK) (23). Central to classical ADCC is the bridging effect facilitated by the antibody, where co-engagement of the structurally distal Fab and Fc results in binding of both the antigenic target as well as the NK cells activating CD16a (FcγRIIIa) receptor, respectively (Fig. 2) (23). If sufficient Fc becomes available following antibody binding to the targeted cell, the recruited NKs will crosslink their Fc-bound CD16a receptors and initiate intracellular pro-cytotoxic pathways: including the release of the

cytotoxic granules perforin and granzyme at the newly formed immune synapse (Fig. 2) (24). Like the C9 component of complement, perforin indirectly drives cytotoxicity by inserting itself into the target cell's membrane (25). This creates an endosomal pore through which granzyme may enter the target's cytosol and directly initiate apoptosis via it's serine protease activity (25). Importantly, this targeted and irreversible destruction of oncogenic cells may prevent the acquisition of drug-resistance that often arises with inhibitory therapeutics, where suppression of one oncogenic signal frequently leads to another's emergence (26). Instead, by directly destroying the cancerous cell, opportunities to acquire resistance are diminished if not all together lost: making ADCC an attractive mechanism for immunotherapeutic exploitation (26). However, a single-nucleotide polymorphism (SNP) at position 158 of CD16a has been shown to dramatically impact ADCC by modifying the FcR's affinity for Fc: being either the high affinity valine (K_D = 0.75 μM) or low affinity phenylalanine (K_D = 5 μM) allotype (27-28). This gives rise to three distinct allotypes, each of which possesses a distinct capacity to facilitate ADCC, where: V/V > V/F > F/F (29). As a result, the majority of ADCC-based therapeutics, including cetuximab, clinically benefit the ≈ 20% of Caucasian patients possessing the high affinity V/V allotype; making the development of strategies that improve Fc binding to the intermediate V/F and low-affinity F/F allotypes of great clinical importance (30).

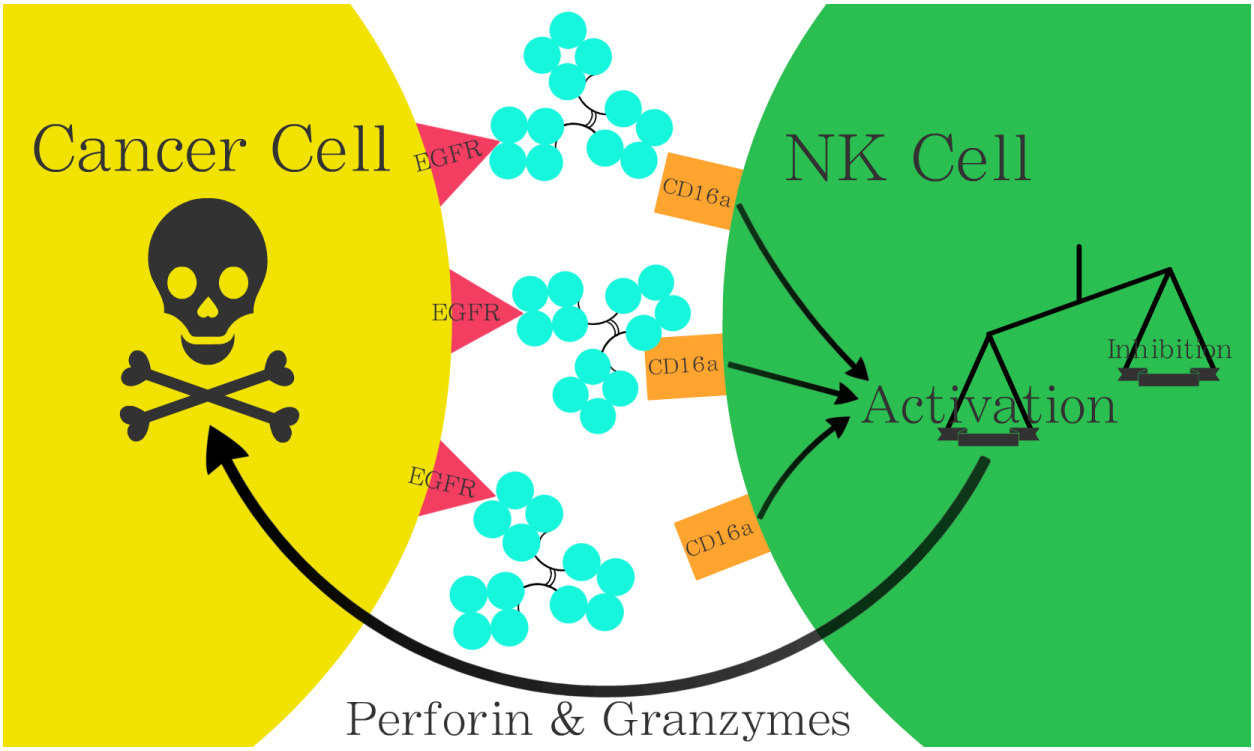

Figure 2: Antibody-dependent cell-mediated cytotoxicity
An EGFR-positive cancer cell is bound by an EGFR specific mAb (e.g. cetuximab), and its exposed Fc recruits nearby NKs by engaging the activating FcR, CD16a. Following sufficient binding of both the antibody to the EGFR and the Fc to NK cell, CD16a cross-linking overrides the NKs inhibitory inputs: shifting the balance in favour of pro-cytotoxic NK cell activation. This activation includes the release of perforin and granzyme: cytotoxic granules that together mediate lysis of the bound cancer cell.

1.3 Augmenting ADCC and reducing V158F allotypic specificity via Fc-engineering

Historically, attempts to augment ADCC have focused on enhancing an antibody's affinity for antigen through variable domain modification, while neglecting the equally essential Fc (31-32). However, current antibody-engineering strategies have since adopted a more holistic approach by continuing to improve antigenic affinities, while concurrently exploring ways to enhance the Fc-mediated interactions necessary for efficient ADCC, regardless of the CD16a SNP (33). Typically, these enhancements have been achieved through two distinct mechanisms: peptide-engineering via the targeted substitution of specific Fc amino acids or, glyco-engineering of a conserved *N*-linked glycan in the C_H2. Though both strategies similarly enhance ADCC, concerns regarding the potential immunogenicity of peptide-modified variants have been raised since these variants do not occur naturally; unlike the distinct engineered C_H2 glycoforms which persist at low levels (<10%) in human serum (34-35). Furthermore, a mAb's capacity to carryout ADCC appears to be limited, as revealed by the redundancy of combined peptide- *and* glyco-engineering, which has been shown to provide no synergistic augmentation to ADCC (36). For these reasons, this investigation has focused exclusively on Fc-glycoengineering, since incorporating Fc peptide-modifications only introduces unnecessary complications and costs without providing any offsetting benefits.

1.3a Fc-glycoengineering: Through modification of a conserved *N*-linked biantennary oligosaccharide found at Asn297 in the C_H2 domain, affinity and specificity against an Fc-receptor (FcR) of interest can be tailored to fit a desired therapeutic application (34, 37). At this glycan, the presence or absence of distinct residues from its mannosyl-chitobiose

backbone results in more than 30 possible C_H2 glycovariants: not accounting for the more than 400 distinct glycoform pairings between each of the Fc's two C_H2 glycans (Fig. 3a) (34). Importantly, particular glycovariants have been correlated with characteristic changes in effector function, having been shown to augment or inhibit various Fc-mediated responses by modulating the Fc's affinity for distinct FcRs (Fig. 3). For instance, increasing the glycans terminal sialylation results in a loss of both CDC and ADCC by enhancing the Fc's affinity for the inhibitory CD32b (FcγRIIb) FcR (Fig. 3b), while increasing galactosylation conversely augments CDC by improving Fc binding to the C1q component of complement (Fig. 3c) (37). Remarkably, these trends hold when the associated glycovariant is localized to only one of the C_H2s glycans, so long as the Fc is not hemi-glycosylated (i.e. missing the other C_H2 glycan) (38-39). Specific to ADCC, C_H2 glycans lacking a core fucose have been shown to augment this response by strengthening the Fc-CD16a interaction (Fig. 3d) (34, 37, 38-39). More specifically, afucosylated C_H2 glycans have been shown to engage in a unique carbohydrate-carbohydrate interaction with another conserved *N*-linked oligosaccharide found on the CD16a: reinforcing their interaction and amplifying NK activation (27, 40). The clinical importance of this glycoform has since been substantiated through investigations of afucosylated cetuximab, and the anti-HER2 mAb trastuzumab: which exhibited a 3- and 10-fold increase in *in-vitro* ADCC compared to their fucosylated counterparts, respectively (41-42).

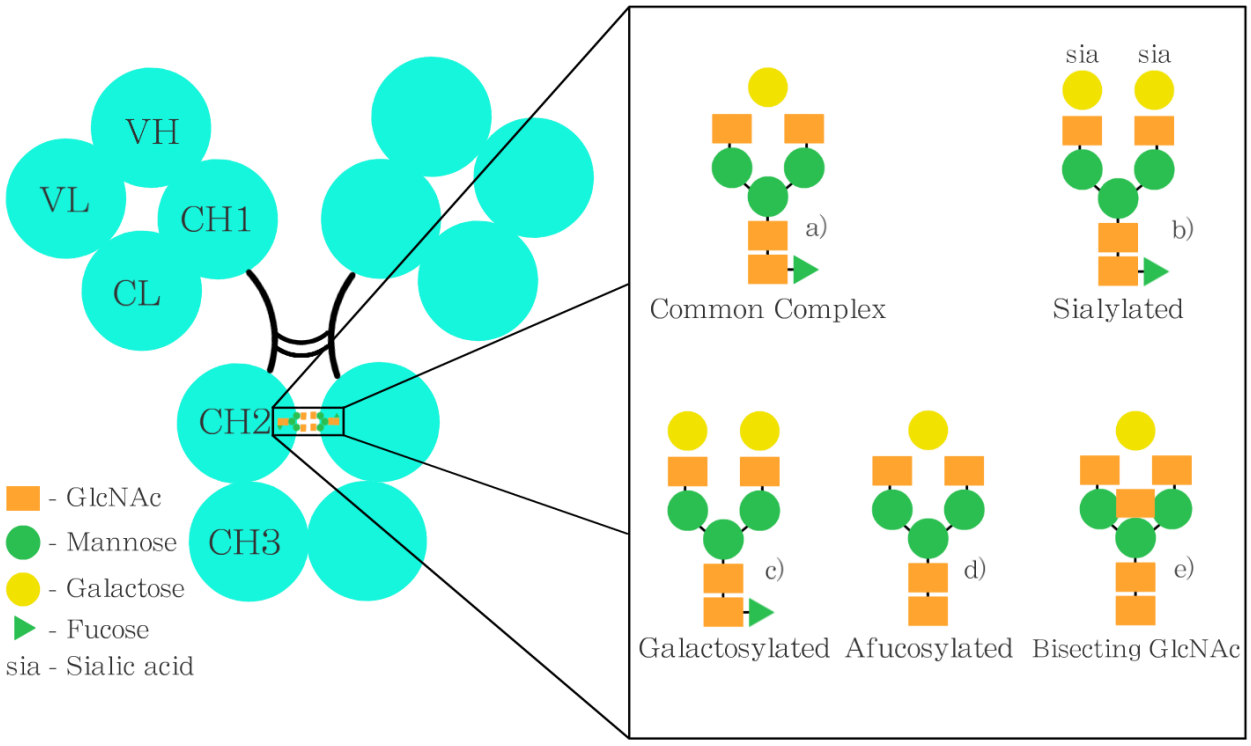

Figure 3: C_H2 glycovariants and their associated effector response

a) Common-complex type glycans make up >90% of C_H2 glycans, and are comprised of the canonical heptasaccharide backbone with variable levels of terminal galactose: being wholly absent or present on one or both of the bi-antennary arms. **b)** <10% C_H2 glycans possess terminal sialic acid (sia): a glycoform associated with an abrogated effector response due to the Fcs increased affinity for the inhibitory NK FcR, CD32b. **c)** Conversely, increased terminal galactosylation has been correlated with an increase in CDC as a result of improved Fc binding to the C1q component of complement. **d)** Specific to ADCC, removal of the basal fucose residue has been shown to enhance Fc binding to the NK activating receptor, CD16a, and augment cytotoxicity. **e)** Similarly, introduction of a bisecting GlcNAc, which may inhibit the enzymatic attachment of the basal fucose, has also been shown to enhance ADCC.

1.3b Strategies to reduce Fc-fucosylation: Asn297 defucosylation can be achieved using a variety of strategies, most of which similarly rely on enzymatically manipulating the glyco-processing pathway (43). Of these, the FUT8- cell line is exceptionally effective since the titular fucosyltransferase, which attaches fucose to the nascent glycan, has been genetically knocked-out (44). Consequent to the lack of FUT8 during mAb expression, this cell line has been shown to reliably produce completely afucosylated glycans: the only intervention reliably boasting this achievement (44). Though unable to reliably achieve true afucosylation, the GnT-III cell line similarly yields high levels of defucosylation by modifying FUT8 activity (45). This is accomplished by overexpressing the titular glucosyltransferase, which results in the addition of a bisecting GlcNAc between the bi-antennary arms of the Asn297 glycan (Fig. 3e) (45). Not typically found at this position, the newly introduced residue is believed to sterically block FUT8 from accessing the glycans basal GlcNAc: preventing the enzymatic addition of a core fucose residue (43, 45). Unfortunately, though both the FUT8- and GnT-III cell lines are widely considered the most reliable methods of achieving highly defucosylated mAbs, they are also proprietary; making their use at smaller production scales prohibitively expensive (46). This has prompted researchers to explore more accessible and affordable alternatives. These include the use of several glyco-processing inhibitors that, when introduced into the expression system, favor the production of the precursor and non-fucosylated high-mannose and hybrid-type glycans (47). Though promising, the resultant glycans are not without issue; often showing significantly higher levels of core fucosylation compared to antibodies derived from the aforementioned cell lines. Additionally, numerous studies have reported that antibodies possessing high-mannose or hybrid-type glycans exhibit short serum retention times, since

their elevated mannose content results in their rapid uptake and clearance by mannose-binding lectins (47-48). To avoid the drawbacks associated with these various cell lines and glyco-processing inhibitors, the enzyme GDP-6-deoxy-D-lyxo-4-hexulose reductase (RMD) has garnered interest as an inexpensive and effective alternative (46). Like the FUT8- and GnT-III systems, RMD treated cells have similarly been shown to produce high levels of non-fucosylated mAbs by disrupting the *de-novo* fucosylation pathway (Fig. 4) (46). Importantly, this is achieved without any costly genetic knockouts or modifications, since RMD can be heterologously expressed in many pre-existing and established mammalian expression systems (46). Following its expression, RMD's oxioreductase activity reduces the 4-keto group of the fucose precursor, GDP-4-keto-6-deoxy-D-mannose, and converts it to GDP-D-rhamnose: a dead-end product which further disrupts fucose production via negative feedback of GMD (Fig. 4). The result of this upstream diversion is a downstream paucity of fucose, with little to none being available for the enzymatic attachment by FUT8 to the nascent Asn297 glycan: resulting in the production of highly defucosylated mAbs (46). With the interest and demand for defucosylated mAbs continuing to rise, researchers are continuing to explore more efficient and less-expensive means of production; this includes the use of RNA inhibitors, as well as intrabodies against the FUT8 enzyme.

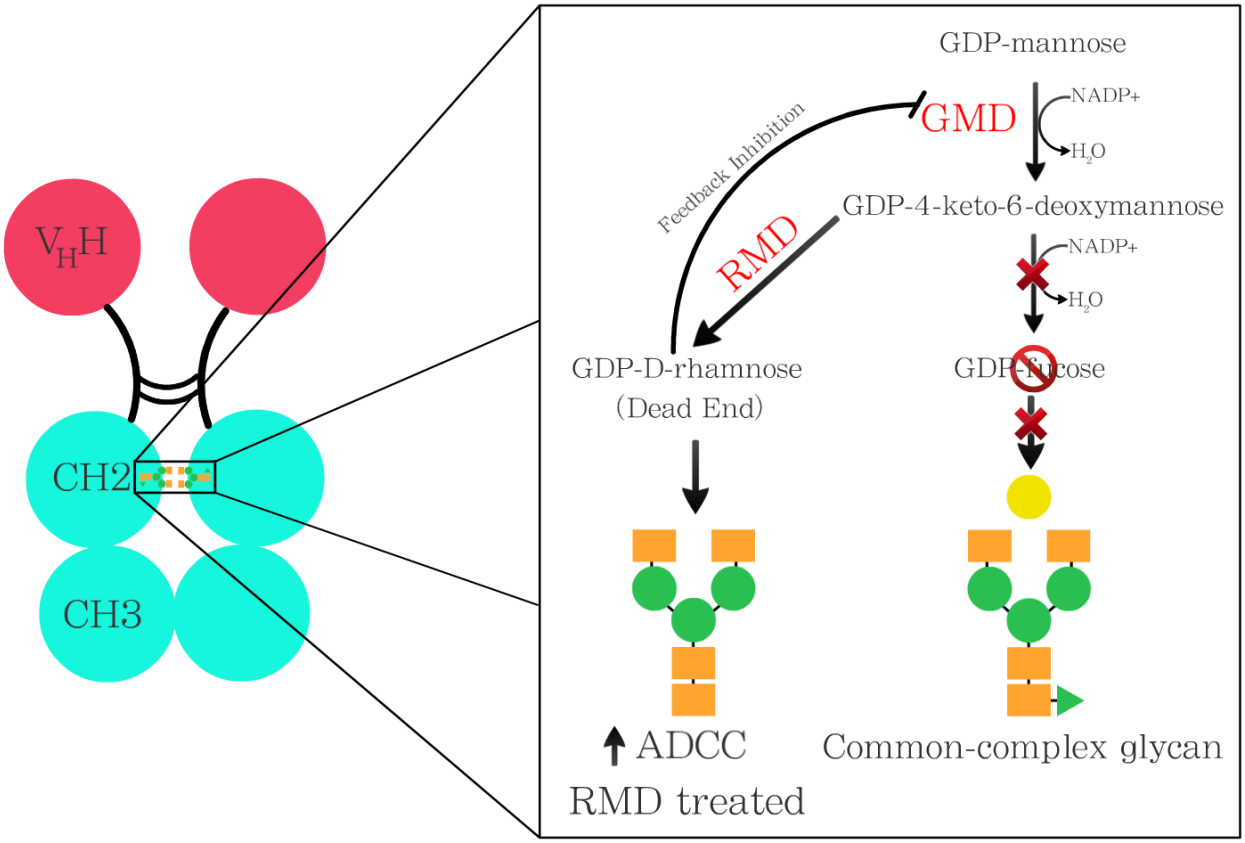

Figure 4: RMD mediated inhibition of the fucosylation pathway
The enzyme GMD actively converts GDP-mannose to GDP-4-keto-6-deoxymannose, which is a GDP-fucose precursor; the residue ultimately added to the nascent Asn297 glycan. When introduced into mammalian cell lines, RMD's oxidoreductase activity diverts GDP-4-keto-6-deoxymannose away from the fucosylation pathway by favouring the production of GDP-D-rhamnose; a dead-end product that further blocks fucosylation by initiating a negative feedback loop with GMD. Together, the diversion and inhibition resulting from RMDs activity creates a paucity of downstream fucose, which can no longer be added to the C_H2 oligosaccharide.

1.4 Variable domain-engineering

1.4a Camelid derived V_HH: Over two decades ago, researchers discovered a novel subset of camelus dromederius (one-humped camel) IgG2 and IgG3, whose structures conflicted with their current understanding of IgG (49). Unlike the tetrameric Fab of conventional IgG, these appropriately titled heavy chain antibodies (HCAbs) were naturally devoid light chains: with antigen-binding domains (ABD) comprised of a lone variable heavy chain (V_HH) (Fig. 1e-f). Despite their initial rarity, HCAbs have since been documented in other camelids, including two-humped camels, llamas and alpacas; along with similar monomeric ABDs derived from distinct species of cartilaginous sharks (50). However, though a high degree of homology exists between camelid V_HH and human V_H, key differences persist; for instance, V_HH often posses an extended CDR3 loop, which is thought to compensate for the missing CDRs typically contributed by the V_L variable domain (50-51). In addition to supporting affinities akin to conventional Abs, this protracted loop is also capable of extending into previously cryptic and inaccessible sites (51). Further differences arise as a result of the missing V_L, whose removal from human IgG1 exposes a hydrophobic V_H face typically buried at the V_H/V_L interface: rendering the IgG unstable (51). However, camelid evolution has overcome this caveat by selecting for V_HHs that possess substitutions that make their V_H interface more hydrophilic: changes that promote V_HH solubility and stability in the absence of V_L (51). Consequently, when expressed independently from the corresponding hinge and Fc, V_HH monomers retain their functionality: making them one of the smallest antigen binding structures presently known (50). In the context of antibody engineering, libraries of monomeric V_HHs specific for an antigen of interest can be generated following the immunization of a camelid with the desired antigenic target (52-

56). Following extraction of cDNA from plasma B cells, monomeric V_HH can be reliably expressed on phage, and subjected to a process known as bio-panning (Fig. 5) (52). This selective process enriches for V_HH exhibiting desirable biophysical properties as determined by their intended application, such as improved affinity, specificity, thermo-stability and solubility (57). For instance, during the selection of V_HH specific for the notoriously resistant gut bacteria *Clostridium difficile*, variants which continued to bind antigen in a high-protease, low-pH environment were selected; enriching for candidates that would likely retain their functionality when exposed to the harsh gut microenvironment following oral administration (52). Furthermore, the production costs of V_HHs are much lower as they can be readily expressed in more unconventional and inexpensive alternatives to animal based systems, including various bacterias (e.g. *E. coli*), yeasts (e.g. *P. pastoris*) and plants (e.g. *A. thaliana*) (58). Collectively, these features have established V_HHs as an important class of therapeutics, whose biophysical pliability and modularity make them ideal building blocks for the assembly of novel antigen binding constructs (50-51).

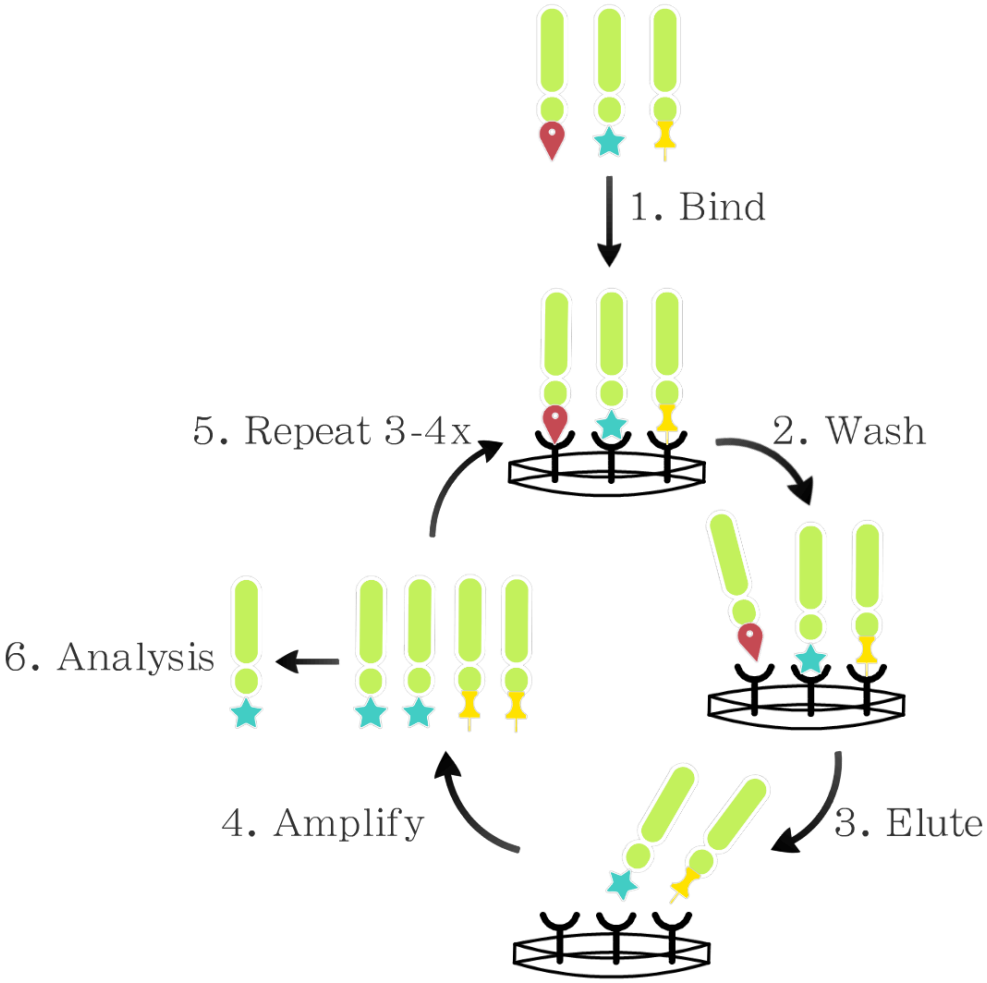

Figure 5: In-vitro affinity selection of V_HH via phage-display
Following immunization, camelid cDNA corresponding to the repertoire of V_HHs developed against the specific immunogen are incorporated and expressed using phage-display technology (1). The phage library is then selected against various antigenic targets, with the option of doing-so under varying conditions (e.g. high heat): "panning" for specific and strong binders while eliminating weak or non-specific binders with washing (2). Any remaining bound variants are then eluted (3), amplified (e.g. *E. coli*) (4) and subjected to repetitions of steps 1-4: enriching for highly specific V_HHs that posses strong affinities and desirable biophysical properties relative to their intended application. (6) At the end of the bio-panning, individual clones are identified by DNA sequencing and binding assays (e.g. phage ELISA).

1.4b Chimeric heavy-chain antibodies: The intrinsically small size of V_HH, arguably their defining feature, offers benefits and drawbacks depending on their intended application; a discrepancy resulting from the fact that their ≈ 13 kDa size falls considerably below the ≈ 60 kDa threshold of glomerular filtration (53). This results in their rapid uptake and clearance by the renal system, yielding serum retention times on the order of minutes (53). If using labeled V_HH for *in-vivo* imaging, this rapid clearance has proven advantageous since the kidneys quickly sequester any unbound V_HH: thus reducing non-specific background "noise" while providing a much clearer image of any labeled masses (53-54). Conversely, V_HH size is a hindrance within a therapeutic context, as their rapid renal uptake fails to provide the time required to exert their biological affect (53). To overcome this, various strategies have been developed: such as introducing the ability to bind canonical serum proteins (e.g. albumin), or linking the V_HH with various peptide backbones or scaffolds in an attempt to increase their size above the renal limit (e.g. PEGylation) (55). Of these options, the hinge-Fc of human IgG1 (hFc) is particularly attractive as it benefits from both of these strategies: prolonging serum retention by increasing the constructs size (≈ 80 kDa), as well as introducing Fc-mediated engagement of the neo-natal FcR (FcRn) and its pH-dependent salvage pathway (Fig. 6) (53, 55). Though hFc addition has proven successful at extending the serum half-lives of V_HH-based constructs from minutes to days, the resultant cHCAbs remain considerably smaller than both conventional mAbs and other novel antigen binding constructs, including scFvs based binders (Fig. 1) (53). Because of this disparity, *in-vivo* imaging has revealed cHCAbs to demonstrate superior tumour penetration and accumulation as a result of their uniquely intermediary size (53). Furthermore, addition of the Fc opens up the possibility for cHCAbs to engage other FcRs,

including the CD16a: the aforementioned NK cell activating receptor integral to anti-tumoural ADCC. However, the therapeutic potential of cHCAbs, including their capacity to facilitate ADCC, remains largely unexplored: underscoring the novelty of this investigation.

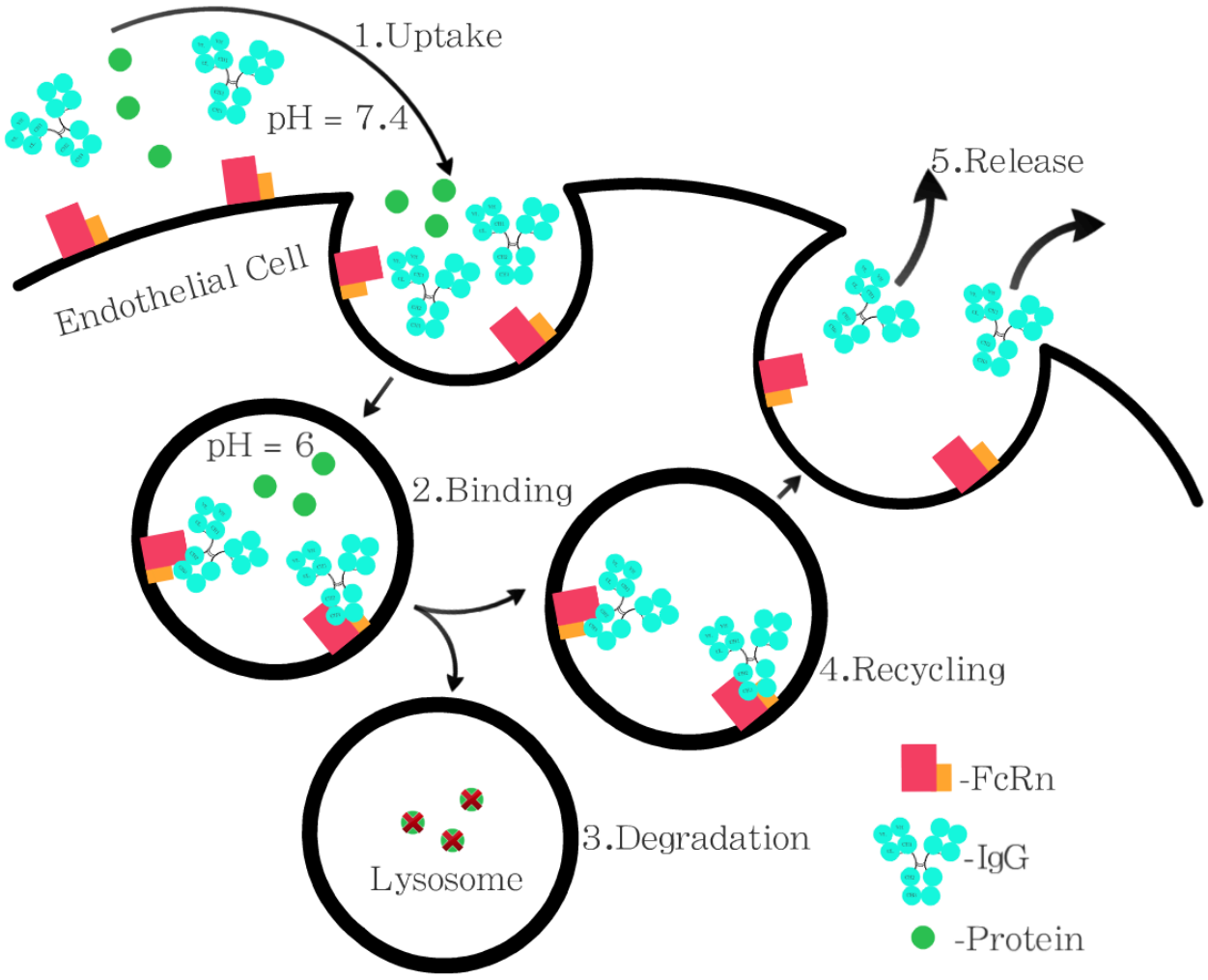

Figure 6: The pH-dependent, FcRn salvage pathway

Circulating Abs and serum proteins are engulfed by FcRn-expressing cells via endosomal-uptake **(1)**. As the endosome begins to bud off into the cytosol, the endosomal pH drops: triggering a pH-dependent interaction between the Ab's Fc and the endosomal FcRn **(2)**. Unlike the unbound proteins **(3)**, this interaction diverts the Abs away from lysosomal degradation **(4)**: eventually returning them, as well as the endosomal FcRn, to the cell surface. Following the endosomes reintegration with the cell membrane, the previously internalized Ab-FcRn complex is again exposed to the extra-cellular pH, which initiates their uncoupling and reintroduces the Abs back into circulation: prolonging their serum retention **(5)**.

1.4c Hinge-engineering: The missing V_L, C_L and C_H1 domains of cHCAbs results in an ABD conformation markedly different from that of IgG1; causing the V_HH arms to be positioned much closer to the centralized Fc (49). Consequently, a cHCAb's ability to interact with its cognate antigen may be constrained to interactions that fail to impart the greatest avidity. For instance, investigation of a distinct V_HH-based construct revealed that decreasing the distance between its bivalent V_HH prohibited their simultaneous binding to antigen; netting an overall loss in avidity (59). Furthermore, the reduced flexibility and distance as a result of this shortening may hinder the cHCAb's ability to assume the asymmetric orientation necessary for efficacious CD16a binding (60). However, such limitations may have been amended over the course of camelid evolution, as naturally occurring long-hinge variants have been found to comprise ≈ 20% of camel-derived HCAbs (61). This distinct subpopulation possesses a 29-35 a.a. long, proline-rich hinge, which together impart length and rigidity: features that have previously been associated with improvements to affinity (62-63, 96). Additionally, previous work has suggested that increasing both hinge length and rigidity should, at the very least, have no detrimental impact on either hFc-CD16a binding or ADCC (64)

1.5 EG2-hFc: a model anti-EGFR chimeric heavy-chain antibody

To investigate the impact antibody engineering has on the anti-tumour activity of cHCAbs, EG2-hFc has been selected as our model construct. The ≈ 80 kDa cHCAb is comprised of a human IgG1 hinge and Fc bivalently linked to EG2: a llama derived V_HH specific for both the EGFR, as well as the truncated EGFRvIII mutant (Fig. 4) (53) Briefly, the EGFR (ErbB-1), along with HER2 (ErbB-2), ErbB-3 and ErbB-4 comprise the ErbB-

family of tyrosine kinase cell surface receptors, which modulate cell growth, migration and proliferation (65). As a consequence of this mitogenic role, EGFR mutations causing receptor overexpression and dysregulation have been linked to a variety of indications: including head, neck, colorectal and breast cancers (66). In such cases, gene amplifications trigger an overexpression of the EGFR at the cell surface, imparting a hyper-responsiveness to mitogenic signals that render the cell oncogenic (Fig. 7) (67). Furthermore, this amplification has also been correlated with the emergence of distinct EGFR mutations: the most common being the EGFRvIII mutant, which has lost the extra-cellular ligand-binding domain (LBD) (68). This truncation further drives tumourigenesis as it results in constitutive EGFR activity in the absence of ligand (Fig. 7) (68). Consequently, EGFRvIIIs extra-cellular alteration, as well as its oncogenic profusion alongside wt EGFR at the cell surface, both act as reliable demarcations between healthy and cancerous-cells; a distinction that is integral to the development of effective cancer-immunotherapies (69). As a result, dysregulated EGFR has become an attractive therapeutic target: leading to the development of EG2-hFc. (65). Though Initially linked to human IgG1 hFc to circumvent the serum retention issues previously described, the bivalent attachment of EG2 also imparts avidity effects believed to give an overall affinity in the low- to sub-nanomlar (nM) range (53). The impact of this avidity was demonstrated *in-vivo*, where EG2-hFc demonstrated superior tumour penetration and accumulation compared to its monomeric counterpart, EG2 (53). Furthermore, linkage to Fc may theoretically permit an anti-EGFR ADCC response; an effector function heretofore unobserved in the context of an EGFR-specific cHCAb. Should any intrinsic cytotoxic response ensue, modifying aspects of the cHCAb's hinge and Fc could augment this, akin to what has been previously reported in

conventional mAbs. In this way, EG2-hFc is being implemented as a representative tool, in an attempt to explore the potential of cHCAbs as a novel anti-tumour therapeutics.

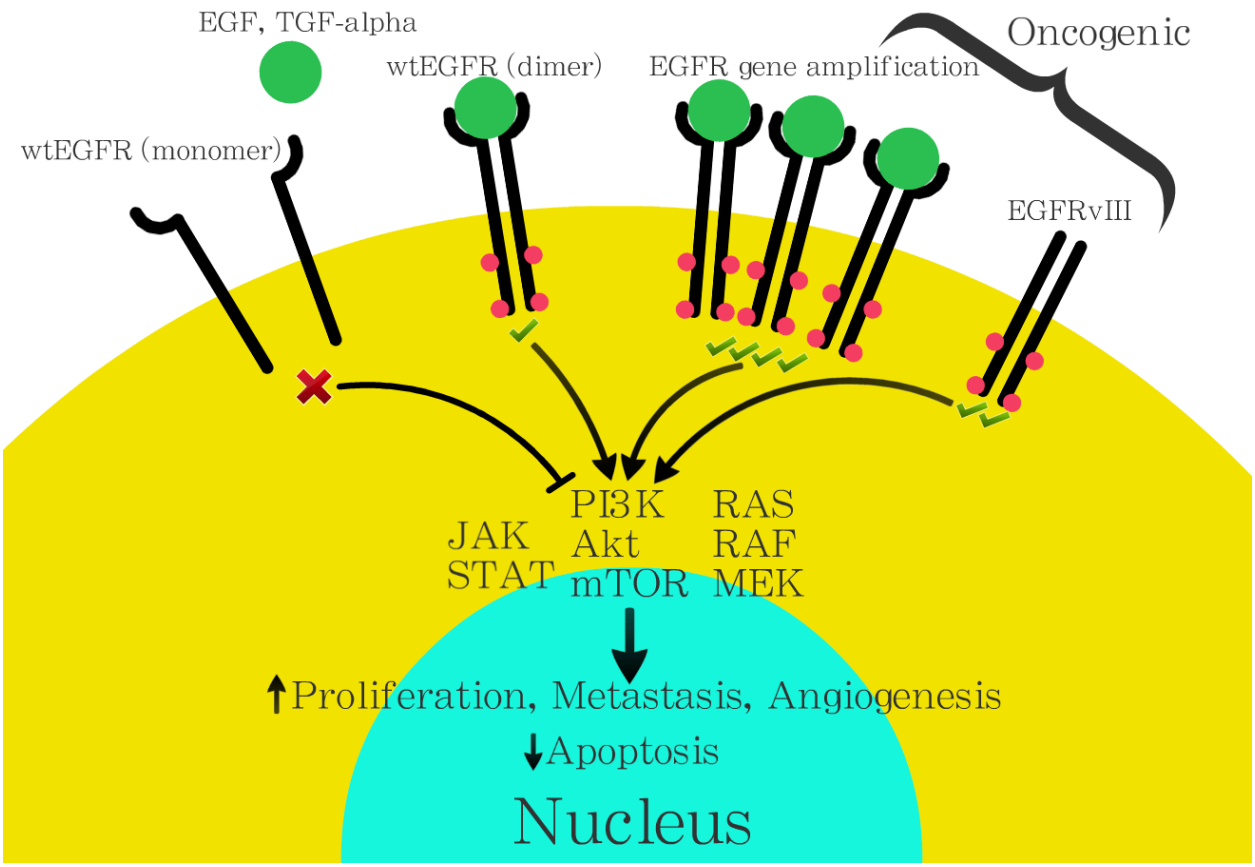

Figure 7: The EGFR (Her1) and EGFRvIII in oncogenesis

Left to right: Upon ligand binding, monomeric EGFR dimerizes: activating the receptors tyrosine kinase activity, and initiating autophosphorylation of the EGFRs intercellular binding domains. This recruits various cytosolic proteins, which when bound, initiate signaling cascades that promote cell proliferation, migration and survival. Various genetic dysregulations have been linked to increased cell surface expression of the EGFR: resulting in an increase of both EGFR dimerization and downstream signaling. Furthermore the EGFRvIII mutation truncates the extracellular ligand-binding domain and renders the receptor constitutively active in the absence ligand. Together, these EGFR malfunctions promote uncontrolled cell growth, proliferation and survival: driving tumourigenesis.

2. Rationale, hypothesis and objectives

2.1 What is missing?

To date, very little is known about the therapeutic potential of cHCAbs, as the initial 2009 EG2-hFc report only explored the constructs use as a diagnostic tool. This current investigation, however, endeavors to address two important questions left unanswered in this preceding study: **can EG2-hFc initiate an anti-tumoural response, and if so, will this be augmented using engineering strategies developed for conventional mAbs?**

2.2 Rationale:

Anti-cancer mAbs developed to interfere with singular steps in various oncogenic pathways typically fail to adequately address the complexities of solid tumours, since the silencing of one oncogenic signal predictably leads to another's emergence. Furthermore, the large size of conventional mAbs is unsuitable within the tortuous solid-tumour microenvironment. Given EG2-hFcs proven capacity for improved tumour-accumulation due to its reduced size coupled with its potential to promote direct killing of cancers cells via ADCC, EG2-hFc may avoid the limitations faced by the current generation of inhibitory mAbs. Should EG2-hFc exhibit any intrinsic ADCC, it may be used as a model cHCAb to investigate whether introducing various glycan and hinge modifications augment it's effector response.

2.3 Hypothesis:

Due to the presence of human Fc, EG2-hFc will facilitate *in-vitro* ADCC of EGFR-positive cancer cells and this response will be modified following Fc and hinge engineering.

2.4 Objectives:

1. Can the cHCAb, EG2-hFc, facilitate ADCC?

1.1 Characterize the intrinsic capacity of EG2-hFc for *in-vitro* ADCC against the EGFR-overexpressing breast cancer cell line MDA-MB-468 using the ^{51}Cr release assay.

2. Will modifying cHCAb hinge-length impact EG2-hFc's effector function and biophysical properties?

2.1 Examine whether modifying the length of EG2-hFc's hinge impacts the cHCAb's ability to facilitate *in-vitro* ADCC.

2.2 Determine whether extending or shortening the hinge of EG2-hFc impacts the cHCAb's thermal stability, aggregation resistance or antigen recognition.

3. Does Fc-glycoengineering augment ADCC by EG2-hFc? Does this modification impact the cHCAbs biophysical properties?

3.1 Characterize whether Asn297 glyco-engineering augments EG2-hFc's ability to facilitate *in-vitro* ADCC.

3.2 Assess the impact Asn297 glycan modification has on EG2-hFc thermal stability, aggregation resistance and antigen recognition.

3. Materials and Methods

Culture of the EGFR-expressing breast cancer cell line: The breast adenocarcinoma cell line MDA-MB-468 (ATCC, Manassas, VA, USA) was kept at 37°C with 60% humidity and 5% CO_2 in RPMI-1640 (Sigma-Alderich, Oakville, ON, Canada) medium supplemented with 10% (v/v) heat-inactivated fetal calf serum (Sigma), 100 µg/mL penicillin (Sigma), 100 µg/mL streptomycin (Sigma). Cells employed in all relevant assays did not exceed 10 passages.

EG2-hFc glycovariants expressed in CHO-3E7: The approved EGFR antibody cetuximab (chimeric IgG1; Erbitux), as well as EG2-X0, EG2- X1, EG2- X2, EG2- X3, EG2-X4, and EG2-X7 were kindly provided by Dr. Yves Durocher (NRC-HHT, Montreal, QC, Canada), and expressed as previously described (70). Notably, during expression of EG2-X7, CHO-3E7 cells were supplemented with 5% RMD to reduce core-fucosylation of the Asn297 glycan.

Construction and expression of EG2-hFc hinge-variants in HEK293-6E cells: HEK293-6E cells were kindly provided by Dr. Yves Durocher (NRC-HHT, Montreal, QC, Canada), and following thawing in 37°C water bath, cells were kept in Freestyle-F17 media (Sigma) supplemented with 10% pluronic acid and geneticin (Gibco, Burlington, ON, Canada) at 37°C in the Multitron PRO incubation-shaker (Infors HT, Anjou, QC, Canada) with 60% humidity, 5% CO_2 and constant shaking at 100 rpm. When 24 h cell doubling coupled with a cell density of 1.5-2 x 10^6/mL was achieved, cells were transfected via PEIpro (Polyplus-transfection SA, Illkirch, France). Briefly, 100 µg of sample DNA mixture was combined with 100 µL PEIpro mixture, pulsed three times, and left to sit for 3 min at room temperature. The mixture was then immediately re-introduced back into the remaining

culture at the above-mentioned conditions. Five days later, cell suspensions were spun at 300 g for 10 min and the collected supernatants put through 0.2 μM filter (Millipore, Etobicoke, Canada). Supernatants were then gravity fed over MabSelect SuRe protein-A affinity columns according to manufacturers instructions (GE Healthcare, Baie-d'Urfé, QC, Canada), and eluted cHCAb fractions were dialyzed against PBS overnight. The following day, cHCAbs concentrations were determined by A_{280} absorbance on Nano-drop 3300 fluorospectrometer (Thermo-scientific, Wilmington, VR, USA), using the molar extinction coefficient of 58,830 for each variant, calculated from their amino acid sequences. 10 μL of each sample was run under reducing (with DTT) and non-reducing SDS-PAGE (Bio-Rad). Finally, all EG2-hFc variants from both CHO-3E7 and HEK293-6E cells, had their Asn297 glycan composition determined by MALDI-MS following treatment with PNGase F (100). Glycan analysis was kindly provided by colleagues at the University of Manitoba, as previously described (100).

Size exclusion chromatography: EG2-hFc variants and cetuximab were passed over a Superdex™ 200 10/30GL (GE Healthcare, Baie-d'Urfé, QC, Canada) size exclusion chromatography column to determine their aggregation state. Briefly, variants were applied at a concentration of 1 mg/mL, with a flow rate of 0.5 mL/min in a mobile phase of PBS (Dulbecco's) under the control of an AKTA™ FPLC (GE Healthcare). To determine each variants size, a standard curve was generated for the Bio-Rad™ Size-Exclusion Chromatography Standard (Hercules, CA, USA) using GraphPad Prism Pro for windows (v6.04, GraphPad software, La Jolla, CA, USA).

CD spectroscopy: EG2-hFc variants were analyzed by CD spectroscopy using a Jasco J-815 spectropolarimeter (Jasco, Easton, PA, USA) at pH 7.4 (100 mM sodium phosphate buffer), as previously described (59). Briefly, a 5-mm cuvette containing 1 mL at 50 μg/mL was used for each sample. Thermal unfolding was followed at 202 nm with CD measurements taken every 0.2°C from 25°C to 96°C with a temperature increase of 1^0C/min. Molar ellipticity ([Θ]) was used to calculate the fraction of protein folded (FF) as follows:

$$[\Theta] = (mdeg \times MRW) \div (pathlength \times [Ab])$$

$$FF = ([\Theta] - [\Theta_F]) \div ([\Theta_F] - [\Theta_U])$$

where mean residue weight, MRW = (molecular weight of the antibody in Da/number of backbone amino acids), pathlength = cell pathlength in mm, and [Ab] = concentration of antibody in mg/mL. Furthermore, $[\Theta_F]$ and $[\Theta_U]$ is the molar ellipticity of the folded (25°C) and unfolded (96°C) states, respectively. Thermal unfolding midpoint temperature (T_m) was obtained by plotting the FF against temperature (T) and fitting with a sigmoidal Boltzman function in Graphpad Prism Pro for windows (v6.04). Three curves were generated for each sample, and the T_m was taken as their average.

Isolation of PBMCs from whole blood samples: Immediately after being drawn, whole blood samples were diluted in half with Dulbecco's PBS (Sigma) and shipped overnight at RT. Once received, 50 mL aliquots were spun at 300 g for 30 min, and buffy coat was removed and diluted 1:1 with PBS. 30 mL of this mixture was then layered over 15 mL Ficoll-Paque PLUS (GE Healthcare), and spun at 300 g for 30 min. PBMCs were then

harvested from the ficoll/serum interface, washed 2x in cRPMI and counted via trypan-blue exclusion. Overnight PBMC cultures were supplemented with 50 units/mL IL-2 in cRPMI and kept at 37°C with 60% humidity and 5% CO_2 until their use on the following day.

***Measure of ADCC via the ^{51}Cr release cytotoxicity assay**:* MD-AMB-468 EGFR+ human breast cancer cells were harvested, washed and labeled with 100 µCi ^{51}Cr (Perkin Elmer, Waltham, MA, USA) in 20 µL FBS in a 37°C water-bath ice until plating. Following 90 min incubation, target cells were washed twice, counted, and placed on ice till plating. During target cell labeling, NK cells were isolated by magnetic negative selection (Miltenyi Biotec, San Diego, CA, USA) from the PBMCs harvested the previous day. Briefly, non-NK cells, i.e., monocytes, granulocytes, T cells and B cells, were magnetically labeled with a cocktail of biotin-conjugated antibodies. Once passed over a magnetic column, the labeled cells were depleted, thus enriching for highly pure NK cells (>90% in all ADCC assays). Purified NK cells were then washed, counted and kept on ice until plating. cRPMI was then added to appropriate wells in a 96-well U-bottom microtest plate (BD Biosciences, Mississauga, ON, Canada) followed by the addition of target and effector cells at the desired E:T ratio. Finally, antibody dilutions were added to appropriate wells giving a final well volume of 200 µL. The 96-well plate was spun for 1 min at 10 g, and placed in an incubator set at 37°C and 5% CO_2 for 4 h. Fifteen minutes prior to completion of incubation, 25 µL of 1% cetrimide was mixed with maximum ^{51}Cr release wells. To account for spontaneous ^{51}Cr release as well as antibody-independent background lysis, control wells were included which contained targets cells with and without NK cells, respectively. Following the 4 h incubation, 50 µL PBS was added to all wells and the plates were spun for 4 min at 10 RCF. Following this

spin, 50 µL of supernatant from each well was transferred and mixed with 150 µL of Optiphase Supermix scintillation fluid (Perkin Elmer) in a 96-well flex-plate (Perkin Elmer). Release of ^{51}Cr was quantified with the 1450 Trilux Liquid Scintillation Counter (Wallac, Waltham, MA, USA, and % specific-lysis was calculated as follows:

*% specific lysis = ((experimental release – spontaneous release)/(maximum release – spontaneous release))*100 – background lysis*

Flow cytometric analysis: Before labeling, all cells were washed with staining buffer (SB) (PBS containing 5% sodium azide). For determination of NK cell purity, cells were labeled on ice for 30 min with Alexa-flour 405-conjugated mouse anti-human CD3 (BD Biosciences) and PE-conjugated mouse anti-human CD56 (BD Biosciences) monoclonal antibodies. Samples were washed again, and run on BD LSRFortessa flow-cytometer running FACSDiva software for windows (BD Biosciences, v6.1.3) following their re-suspension in 0.5 mL SB. For indirect immunofluoresence of EGFR binding by EG2-hFc variants, MDA-MB-468 cells were washed in SB, then incubated with various concentrations of EG2-hFc variants. Following a second wash, target cells were stained with the IgG1 Fc-specific FITC-conjugated mouse anti-human IgG mAb (Sigma) for 30 min on ice. Samples were then washed and re-suspended in 0.5 mL SB, then run on BD LSRFortessa flow-cytometer. All flow-cytometric analysis, including determination of median-fluoresence intensity, was done with FlowJo for windows (v7.6.5. FlowJo LLC, Oregon, USA)

Flow-cytometric determination of CD16a allotype: A fraction of each PBMC sample received was washed and labeled in ice-cold staining buffer with mouse anti-human: CD56-

PE, CD3-AF405, and either 3G8-FITC or MEM154-FITC (both anti-CD16a) for 30 min on ice. Samples were washed and re-suspended in 0.5 mL staining buffer and run on LSRFortessa flow-cytometer (BD). Analysis was done using FloJo software.

Data processing and statistical analysis: Data are displayed graphically and were statistically analyzed using Graphpad Prism Pro for windows (v6.04). Curves were fitted using a nonlinear regression model with a sigmoidal dose response (variable slope). The respective results are displayed as mean ± SEM, unless stated otherwise.

4. Results

4.1 Expression and biophysical characterization of the EG2-hFc variants

4.1a EG2-hFc expression using distinct mammalian cell lines: EG2-X0, EG2-X1 (CHO), EG2-X2 and EG2-X7 were all expressed using the CHO-3E7 cell line by Dr. Yves Durocher (Fig. 12) (70). The remaining variants, EG2-X1 (HEK), EG2-X5 and EG2-X6, were expressed in the non-adherent HEK293-6E cell line using the pTT5 vector (Fig. 12). Following their successful expression, reducing and non-reducing SDS-PAGE gel-electrophoresis of the HEK293-6E expressed variants revealed bands corresponding to the expected molecular mass of the dimerized (≈ 80-90 kDa) and monomeric (≈ 40 kDa) cHCAb chains (Fig. 9). SEC analysis revealed no aggregation across all variants, with the exception of EG2-X0 and long-hinge EG2-X6, which both exhibited small peaks corresponding to the formation of high molecular weight aggregates (Fig. 10). EG2-X6 also eluted earlier than expected, giving a mass estimate (≈ 120 kDa) that was considerably different from estimates predicted from both its a.a. sequence, as well the preceding SDS-PAGE analysis.

4.1b EG2-hFc glycosylation profiles: In agreement with the wealth of information regarding clinically available cetuximab, the mouse-human chimeric mAb we employed was predominantly complex-type with variable galactosylation (Fig. 12). Amongst the EG2-hFc variants, despite our concerns that differences in glycosylation could result from the use of two distinct expression systems, both CHO-3E7 and HEK293-6E produced similar glycovariants possessing highly galatosylated, complex-type glycans; save for the RMD treated EG2-X7 which showed a 25% reduction in overall core fucosylation (Fig. 12).

4.1c EG2-hFc hinge modifications: EG2-X2, EG2-X5 and EG2-X6 all underwent hinge modification, with EG2-X2 and EG2-X5 both lacking the IgG1 upper-hinge cysteine pairs, while EG2-X6 possessed a camelid derived long-hinge (Fig. 8, 12). Importantly, the upper-hinge cysteines were removed from EG2-X2 and EG2-X5 via two distinct means; with the former having a large portion of the hinge containing the cysteines excised, while the latter had the cysteines replaced with serines (Fig. 8). Finally, a naturally occurring 35 a.a. long hinge was introduced into EG2-X6 in order to extend the distance between the EG2 ABDs (Fig. 8, 12).

4.1d Thermo-stability of EG2-hFc variants: Circular dichroism was used to determine the thermal-unfolding midpoint (T_ms) of the EG2-hFc variants. Initially, the original EG2-X0 demonstrated a biphasic curve: with an initial unfolding around 50°C followed by another at 72°C (Fig. 11a). Subsequent sequence analysis revealed EG2-X0 to contain two unintended mutations in the Fc: D270G and Y278H (Fig. 8). In order to ascertain the respective impact of both these mutations, each was individually introduced and expressed in human IgG1 Fc (Fig. 8). Subsequent CD analysis of the mutated Fcs, hFc-X3 (D270G) and hFc-X4 (Y278H), revealed them both to exhibit a biphasic-unfolding curve akin to EG2-X0 (Fig. 11g-h). When the mutated Fc of EG2-X0 was replaced with the wt Fc of IgG1, the expected monophasic-melting curve was restored with EG2-X1 (Fig 11b). All subsequently expressed hinge- and glycovariants possessed the wt IgG1 hFc, and demonstrated the characteristic mono-phasic unfolding, with T_ms ranged from 71-75°C (Fig. 11b-f).

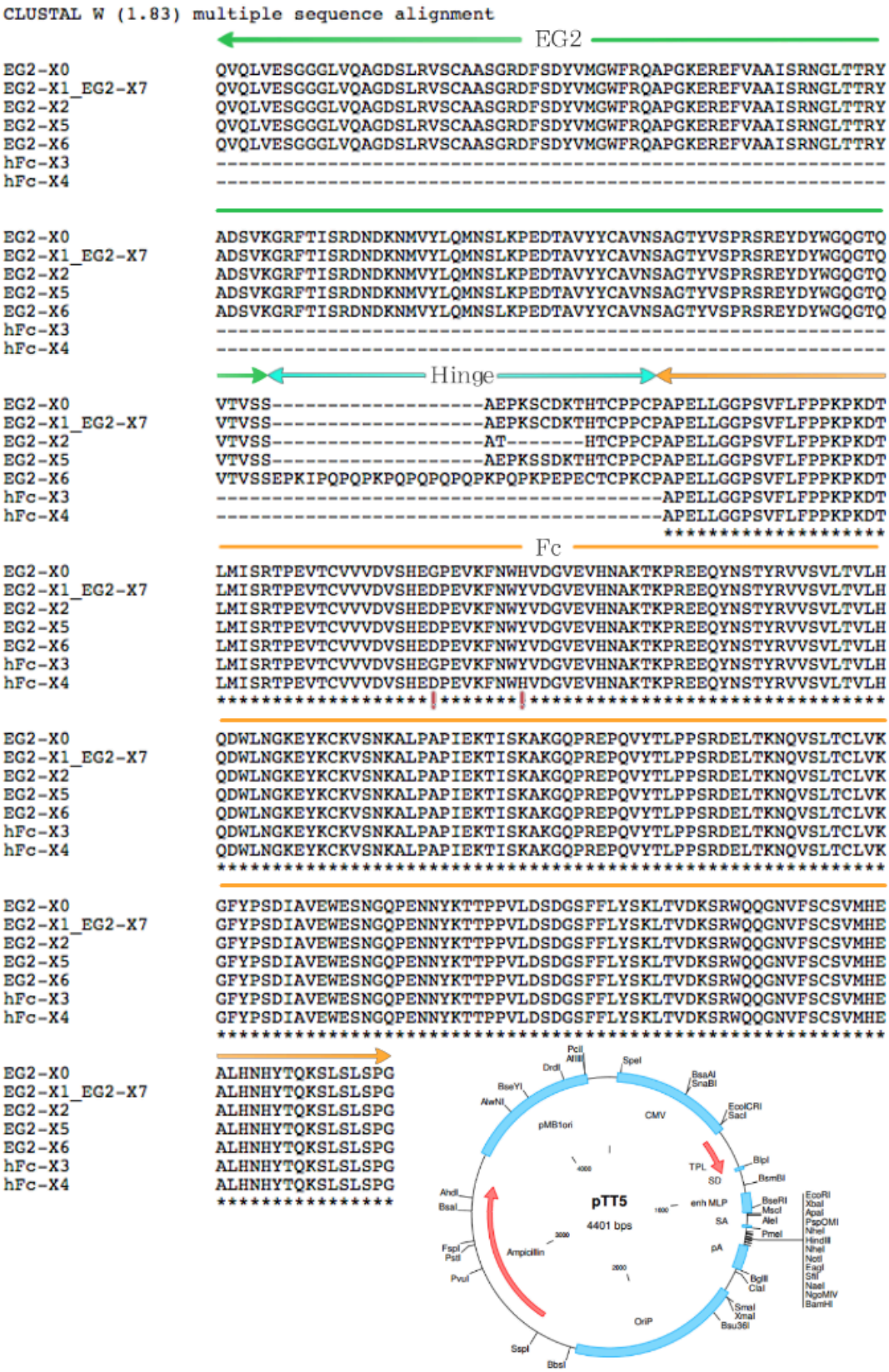

Figure 8: Amino acid sequences of EG2-hFc variants and the pTT5 expression vector

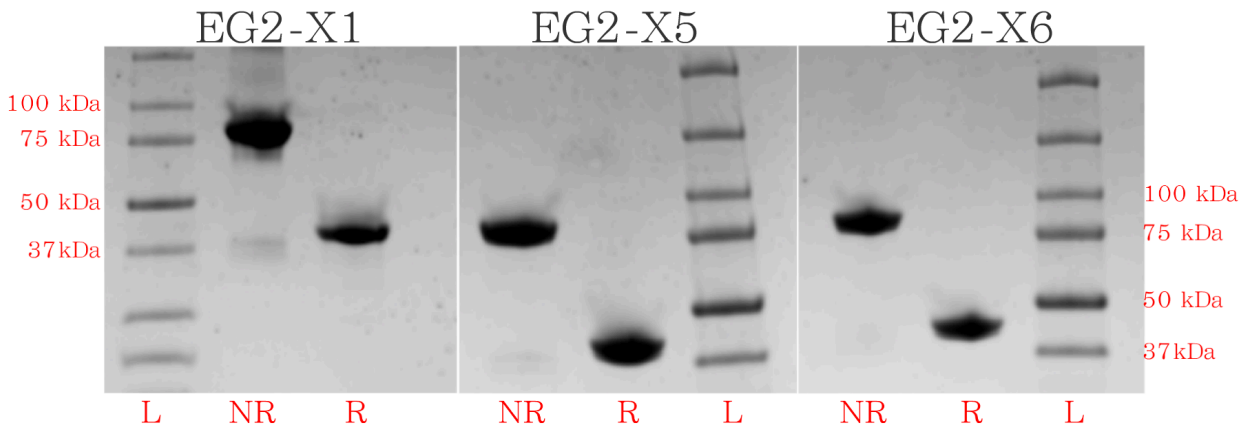

Figure 9: SDS-PAGE of HEK293-6E expressed EG2-hFc variants

Each of the HEK293-6E expressed EG2-hFc variants revealed prominent bands corresponding to their monomeric (≈ 40 kDa) and dimerized (≈ 80-90 kDa) chains, under reducing (R) and non-reducing (NR) conditions. Faint bands corresponding to unpaired monomers were detected for both EG2-X1 and EG2-X5 under non-reducing conditions.

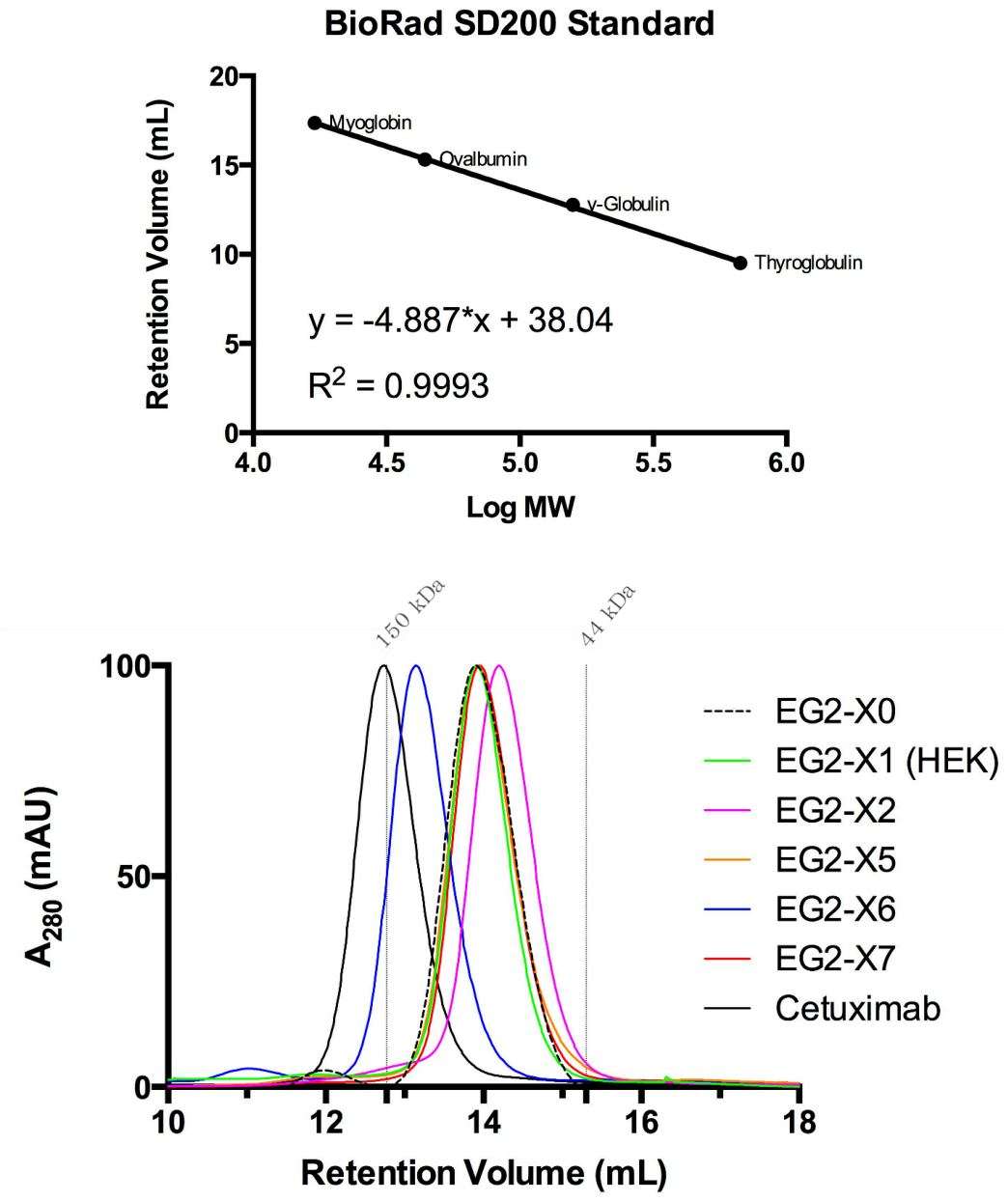

Figure 10: Size exclusion chromatography of EG2-hFc variants and cetuximab

Separations were carried out over a Superdex 200™ column in PBS. **Top:** BioRad chromatography protein standard was run over the column to allow for the estimation of molecular weights of EG2-hFc variants. **Bottom:** Based on predicted sizes, EG2-hFc variants and cetuximab eluted as expected. However, long-hinge EG2-X6 eluted faster than expected, giving a mass estimation (120 kDa) which differs from the SDS-PAGE estimated mass (90 kDa). Vertical lines indicate elution positions of γ-globulin (158 kDa) and ovalbumin (44 kDa). Data is normalized to a maximum 100 milliabsorbance units.

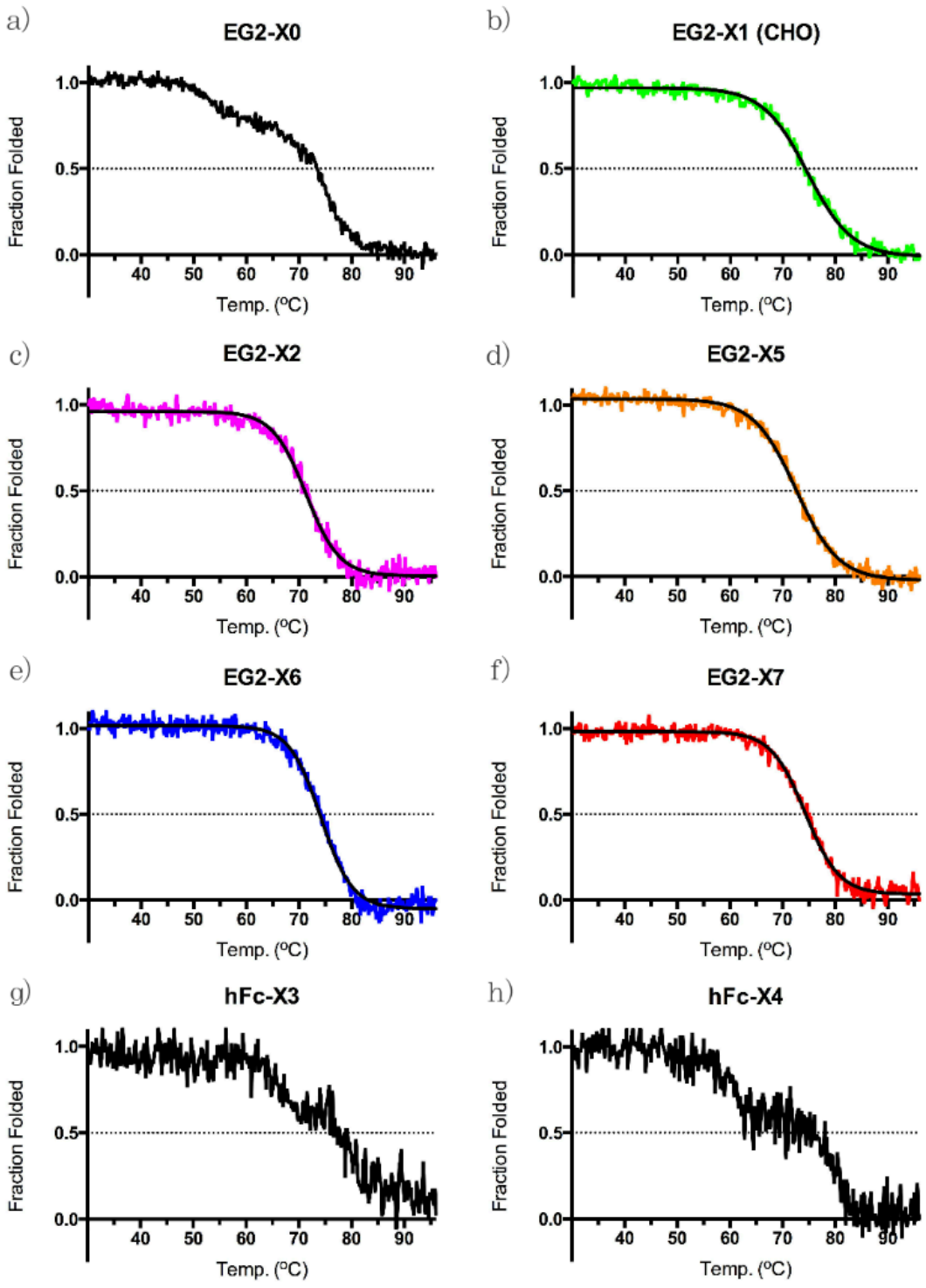

Figure 11: T_m Determination of the EG2-hFc variants and Fc-mutants

For specific T_m values, see figure 12.

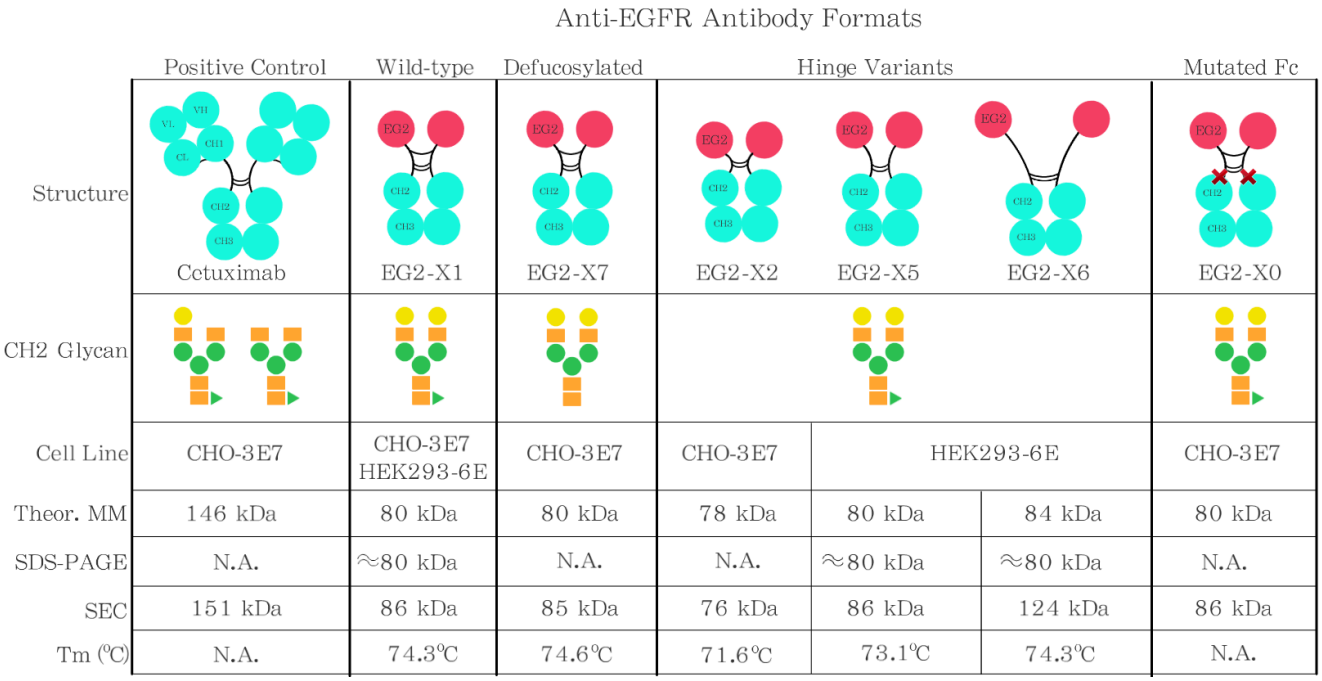

Figure 12: Summary of cetuximab and EG2-hFc variant biophysical properties

The clinically available glycovariant of the mouse-human chimeric mAb cetuximab is predominantly complex-type with variable galactosylation. Conversely, each of the CHO-3E7 and HEK293-6E expressed EG2-hFc variants possessed highly galactosylated complex-type glycans, save for the RMD treated reduced-fucose EG2-X7. EG2-X2, EG2-X5 and EG2-X6 all posses a modified IgG1 hinge: with EG2-X2 and EG2-X5 both lacking the upper-hinge cysteine pair, and EG2-X6 possessing a camelid derived long-hinge. Additionally, all cHCAb, including the elongated EG2-X6, exhibit sizes smaller than cetuximab as revealed by SEC and SDS-PAGE.

4.2 Flow-based characterization of EGFR binding by EG2-hFc variants: Flow-cytometry was used to ensure that each EG2-hFc variant retained the ability to bind cell-surface EGFR, regardless of the various modifications that had been introduced. All EG2-hFc variants, as well as cetuximab, were tested at various concentrations against the EGFR-positive breast cancer cell line MDA-MB-468, and binding was indirectly detected with the use of goat anti-human IgG1 (Fc-specific) FITC-conjugated mAb (Fig. 13). Comparable binding profiles were observed for wild-type EG2-X1, serine-replaced EG2-X5 and the glycoengineered EG2-X7 variants (Fig. 13a,c,e). Dissimilarly, the truncated and long hinge variants, EG2-X6 (Fig.12d) and EG2-X2 (Fig.13b), deviated from the remaining variants by exhibiting the highest and lowest MFI values, respectively; indicating that hinge length or composition impacts EG2-hFc's ability to bind cell-surface EGFR. A K_D value of 0.38 nM was derived from cetuximab's binding profile, which is in agreement with affinity values reported elsewhere (80). Unfortunately, because each EG2-hFc variant required unfeasibly high concentrations in order to achieve saturating EGFR binding, their K_D values could not be estimated. Interestingly, no EGFR-binding by EG2-X0 could be detected using the Fc-specific FITC-conjugated secondary antibody (data not shown. This observation served as an early indicator that the Fc of EG2-X0 was in some way atypical: prompting the investigation that led to the discovery of the Fc mutations, D70G and Y278H (Fig. 8).

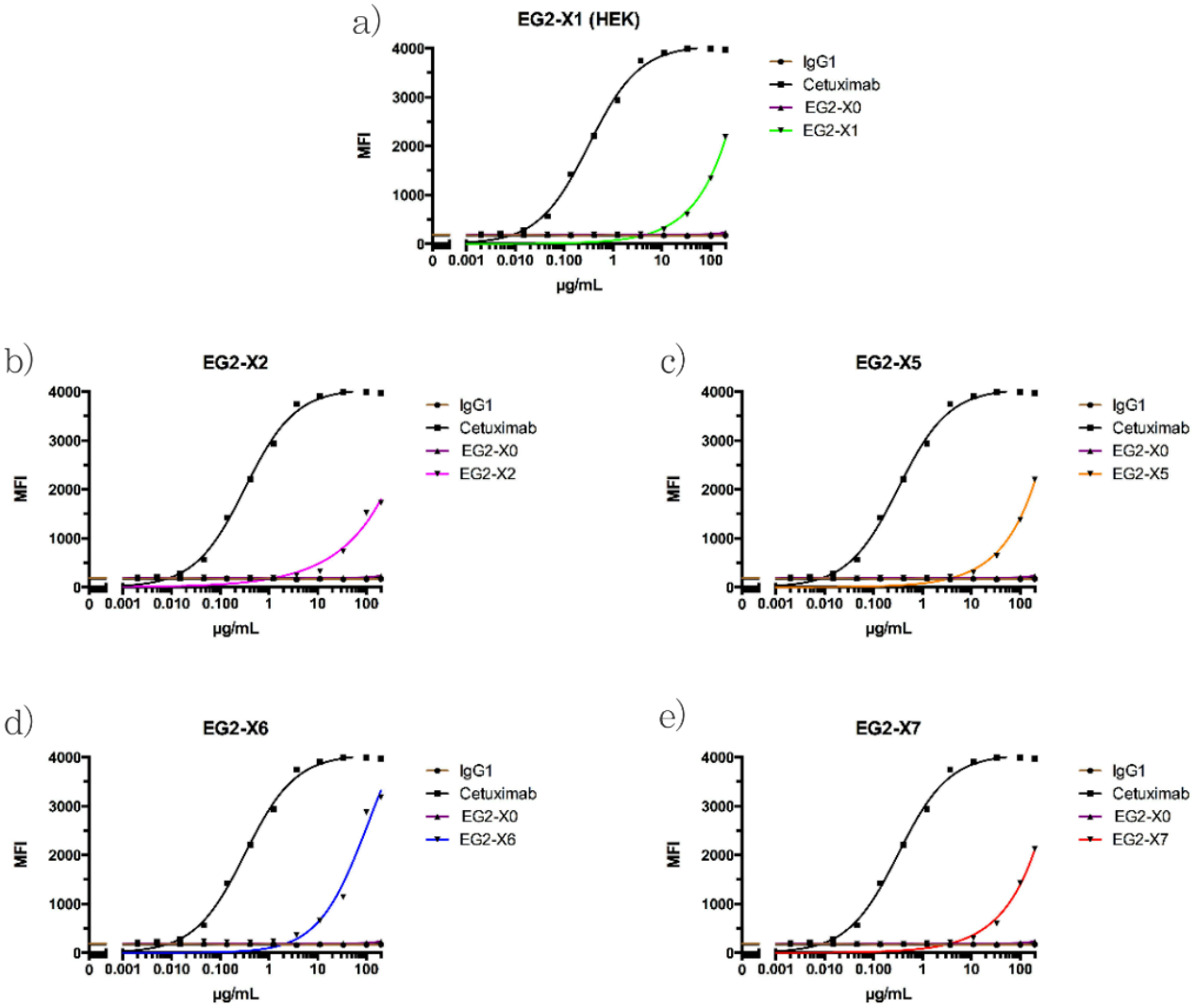

Figure 13: Flow-based determination of EG2-hFc binding to cellular EGFR

All EG2-hFc demonstrated clear binding to the EGFR-positive breast cancer cell line, MDA-MB-468: however, saturating binding could not be achieved for the EG2-hFc variants, which prevented calculation of their K_D. EG2-X1 **(a)**, EG2-X7 **(e)** and serine-replaced EG2-X5, all of which possess nearly identical hinges, exhibited similar binding profiles. Conversely, the short-hinge EG2-X2 **(b)** and long-hinge EG2-X6 **(d)** showed the weakest and strongest MFIs, respectively. MFI was derived using FlowJo software, and graphed using GraphPad prism Pro (v6.04).

4.3 Optimization of the ^{51}Cr release assay using primary NK cells: Due to the difficulties associated with the use of primary NK cells, determining the minimum number of cells required to generate an unambiguous ADCC signal was of great importance. To establish this, initial CRAs were used to determine both the minimal effector to target ratio (E:T) and concentration of cetuximab required to provide a clear ADCC signal. As figure 14 indicates, E:T ratios of 100:1 and 50:1 provided the strongest lytic signals; however subsequent assays revealed that achieving the required numbers of NK cells was unfeasible. Instead, the E:T ratio of 10:1 was selected as it, along with a starting cetuximab concentration of 0.2 μg/mL, provided a clear ADCC signal, while requiring a minimal amount NK cells and cetuximab (Fig. 14). Furthermore, these parameters also exhibited low levels (≈ 10%) of background antibody-*independent* killing (Fig. 14). Moving forward, this E:T and concentration of cetuximab were selected for subsequent CRAs. Furthermore, NK cell stimulation with IL-2 was limited to less than 15 hours, as overstimulation led to sharp increases in background antibody-*independent* killing; skewing interpretation of specific lysis data.

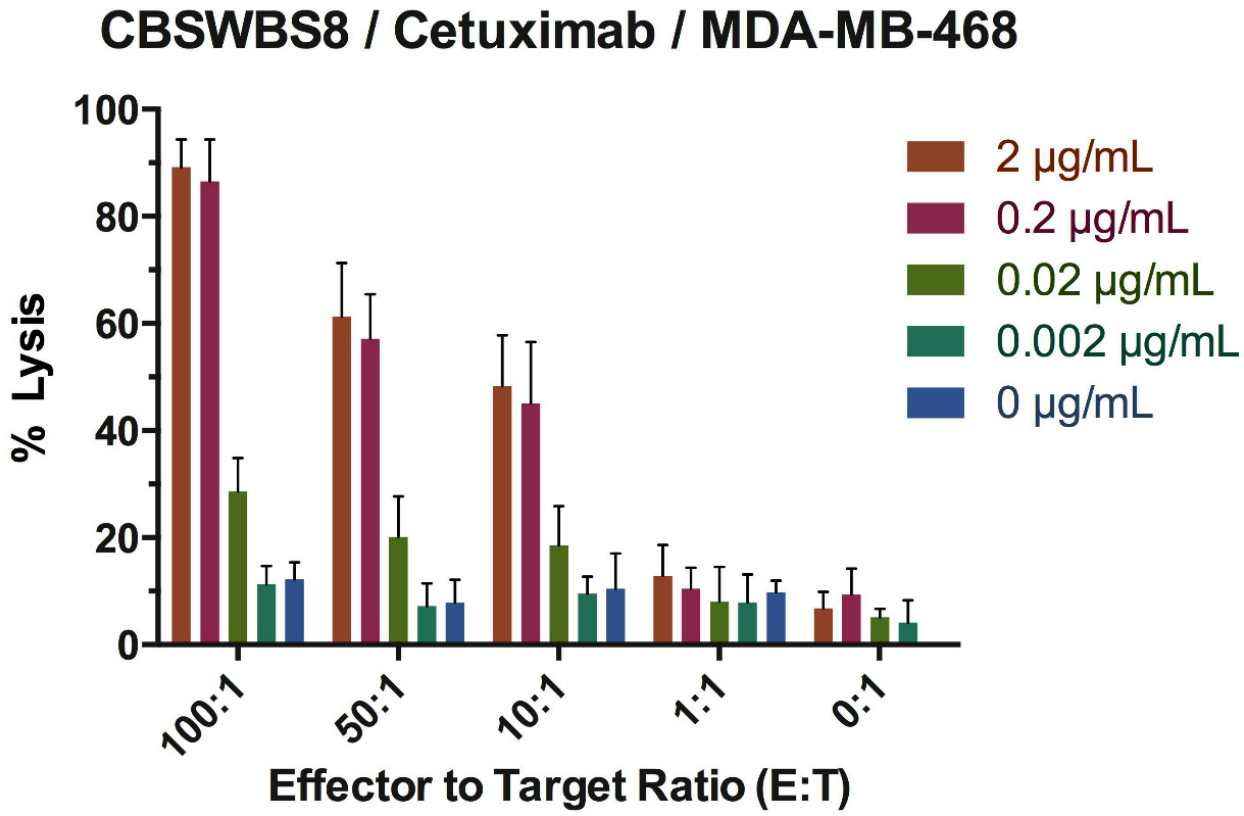

Figure 14: Optimization of the ^{51}Cr release assay

The percent of lysis of tumour cells (MDA-MB-468) as a function of E:T ratio and cetuximab concentration, is shown. Data are presented as mean ± SD of triplicate wells from a single experiment with the corresponding NK cell donor (CBSWB8). For this, and all subsequent ADCC assays, a >90% purity of $CD16^{+}$:$CD56^{+}$;$CD3^{-}$ NK cells was achieved, as determined by flow-cytometry.

4.4 Characterization of EG2-X0 and its associated glycovariants: Characterization of EG2-X0, the original EG2-hFc variant from the 2009 study, revealed it's failure to initiate detectable ADCC (Fig. 14,15a); an observation subsequently linked to two then unknown Fc mutations. With this revelation yet to be uncovered, it was postulated that EG2-X0 might be facilitating low-levels of ADCC that were indistinguishable from background lysis. To address this, EG2-X0 underwent Fc-glycoengineering in an attempt to augment any low-levels of intrinsic ADCC that may be occurring: thereby boosting the lytic signal into a detectable range. Three glyco-processing inhibitors were used to generate EG2-X0 with reduced Asn297 fucosylation: kifunensine, swainsonine and castanospermine, all of which function by halting the glyco-processing pathway before Asn297 fucosylation can occur. This results in the production of hybrid and high-mannose type glycans, which lack core fucosylation. Despite these efforts, the resultant EG2-X0 glycovariants, EG2-Kif, EG2-Swain and EG2-Cat, all failed to exhibit ADCC (Fig. 15): further confirming EG2-X0's inability to initiate ADCC.

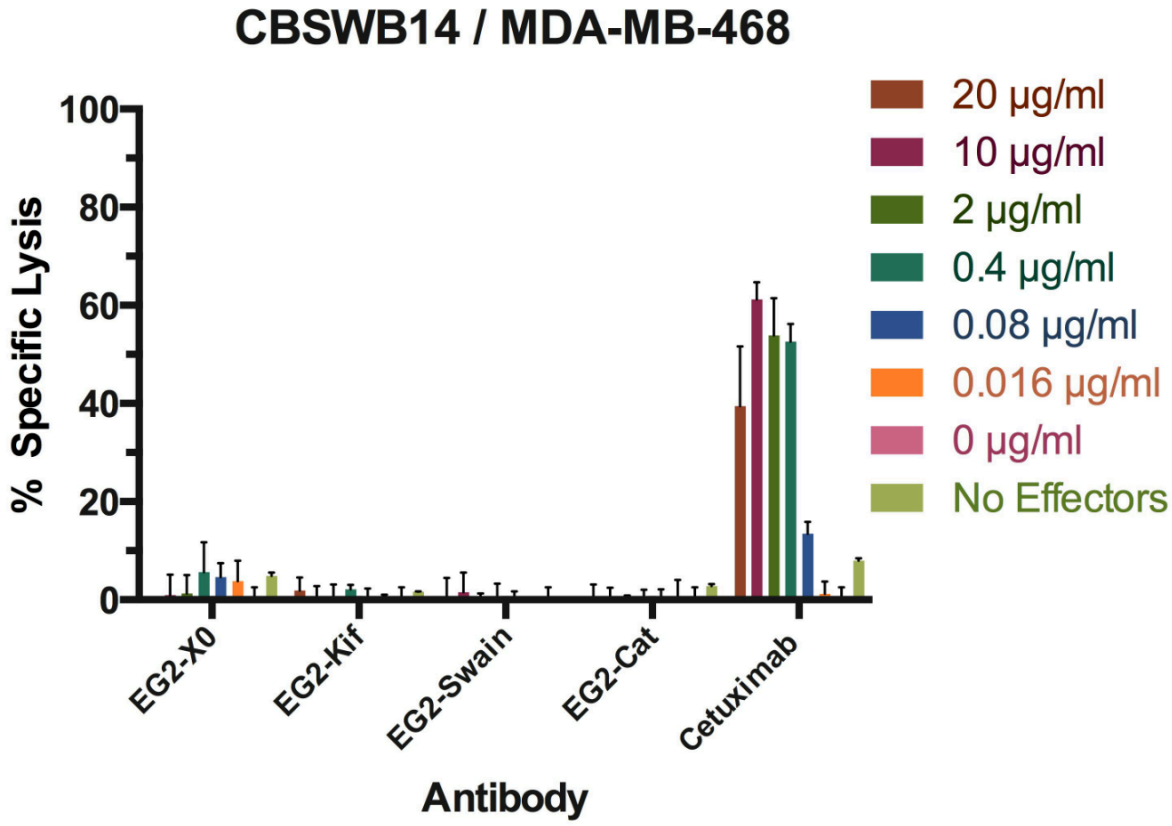

Figure 15: EG2-X0 and it's associated Fc-glycoengineered variants fail to initiate ADCC

Cetuximab facilitated clear ADCC against the target cell line, while EG2-X0 and its associated glycovariants all failed to initiate any significant lysis. Data are presented as mean ± SEM of triplicate wells from a single experiment with the corresponding NK cell donor (CBSWB14).

4.5 ADCC by EG2-X1 following reversion of Fc mutations: In response to the discovery of the mutated Fc of EG2-X0, the problematic Fc was replaced with wt Fc of human IgG1, giving EG2-X1. Following this correction, ADCC was restored for EG2-X1; the first documented effector response by an EGFR-specific cHCAb (Fig. 16b). To ensure that no differences in ADCC would result from our use of two distinct expression systems, EG2-X1 was expressed in both CH0-3E7 and HEK293-6E cell lines. The two resulting EG2-X1 variants mediated similar levels of ADCC when characterized using the same NK sample: indicating that our use of two distinct mammalian expression systems would not result in disparate ADCC profiles (Fig. 16c,d).

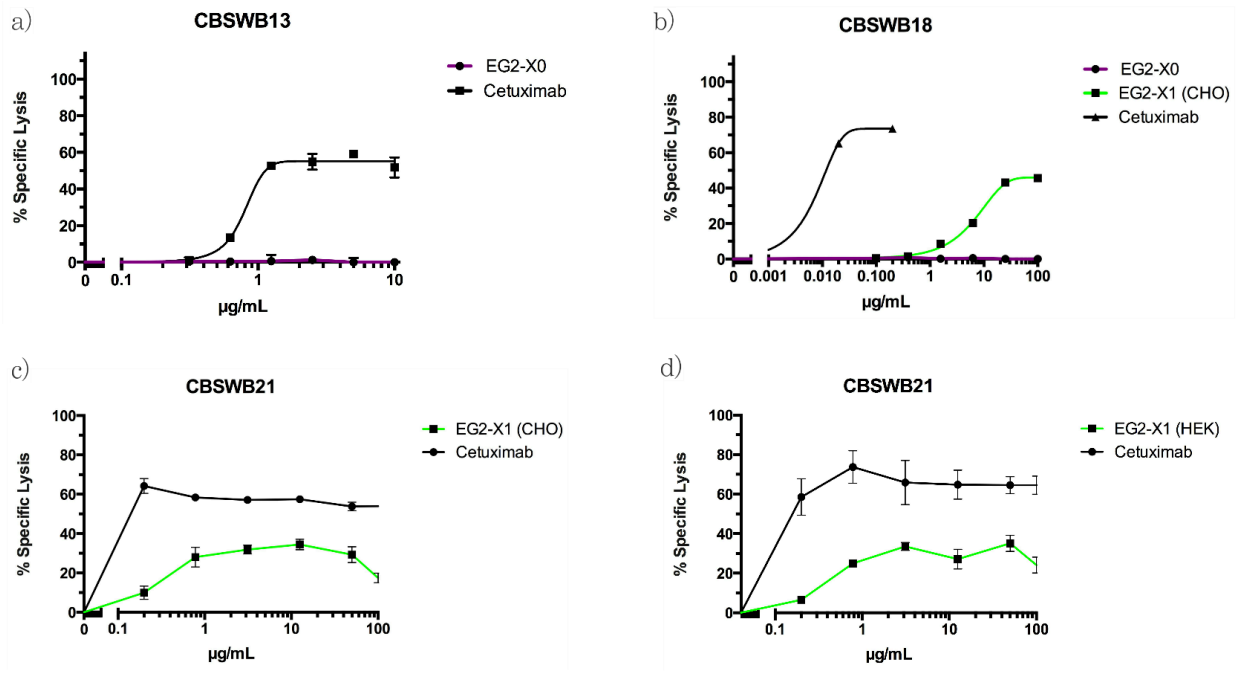

Figure 16: Recovery of ADCC following reversion of EG2-X0 Fc mutations

The failure of ADCC exhibited by EG2-X0 (a) was reversed following the reversion of the two Fc mutations, D270G and Y278H (b). To ensure no differences in EG2-hFc functionality resulted from our use of two distinct expression systems, EG2-X1 was expressed in both CHO-3E7 (c) and HEK293-6E (d), and both variants exhibited similar ADCC profiles. Data are presented as mean ± SEM of triplicate wells from individual experiments with the corresponding NK cell donor (CBSWB13, 18, 21).

4.6 Preliminary ranking of ADCC by EG2-hFc variants: Following the successful ADCC by EG2-X1, a preliminary ranking of both HEK293-6E and CHO-3E7 derived EG2-hFc variants was completed (Fig. 17). Of these, long-hinge EG2-X6 (Fig. 17c) and de-fucosylated EG2-X7 (Fig. 17d) showed the greatest overall ADCC relative to cetuximab, while the serine-modified EG2-X5 (Fig. 17b) showed lysis similar to unmodified EG2-X1. Finally, the short-hinge EG2-X2 showed no ADCC (Fig. 17a), establishing a hierarchy that would persist throughout the ensuing battery of CRAs, where: EG2-X6 ≥ EG2-X7 > EG2-X5 = EG2-X1 >> EG2-X2 = EG2-X0.

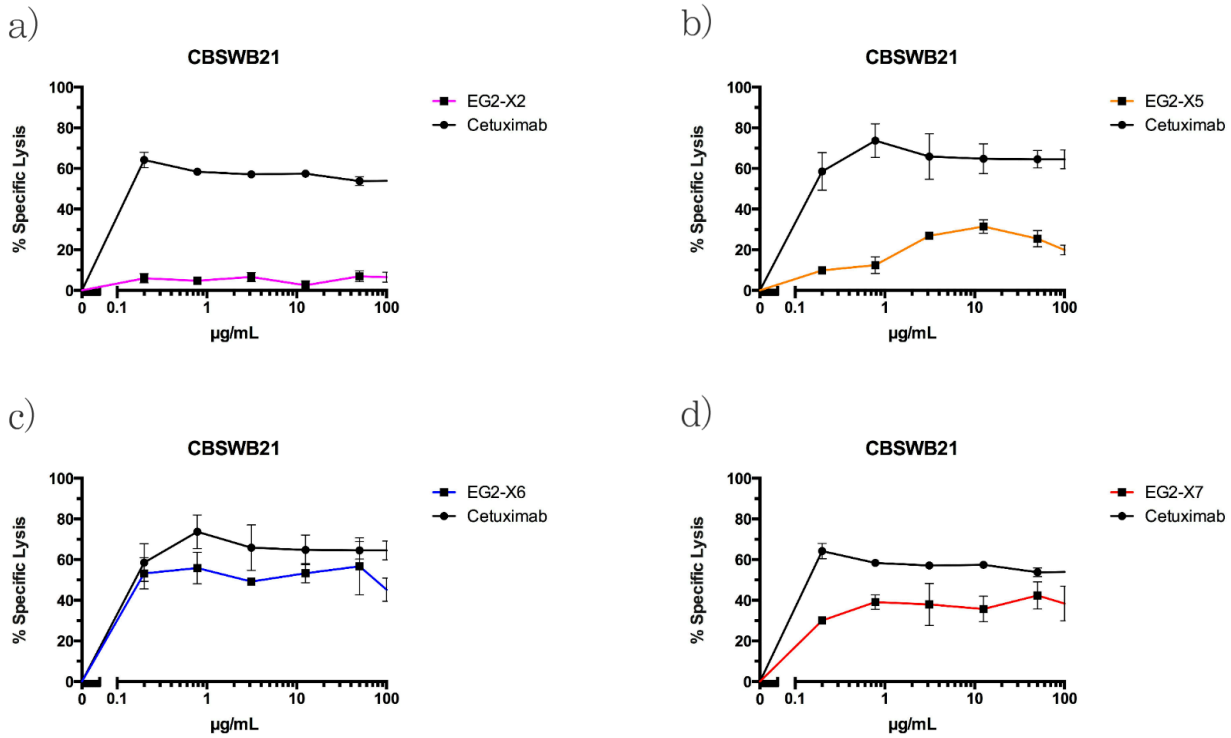

Figure 17: Preliminary ADCC ranking of EG2-hFc hinge and glycovariants

Like the mutated EG2-X0, the short-hinge variant, EG2-X2 (a) similarly failed to initiate ADCC, while the serine-replaced hinge-variant EG2-X5 (b), demonstrated lysis similar to EG2-X1. The long-hinge EG2-X6 (c) exhibited the greatest degree of lysis while the Fc-glycoengineered EG2-X7 showed a slightly lower response, relative to cetuximab. Data are presented as mean ± SEM of triplicate wells from individual experiments with the corresponding NK cell donor (CBSWB21).

***4.7 Impact of hinge-modification on ADCC by EG2-hFc*:** Short-hinge EG2-X2, which had a portion of it's upper-hinge excised, which included the cysteine pair in question, repeatedly failed to show any ADCC across multiple NK cell samples (Fig. 18a-c). The serine-modified EG2-X5, which retained the hinge-length of a typical IgG1 but similarly lacked the pair of upper-hinge cysteines, exhibited ADCC akin to unmodified EG2-X1 across multiple NK cell samples (Fig.19a-c). Finally, the long-hinge EG2-X6 repeatedly demonstrated greater overall lysis compared to both of the hinge-variants, as well as unmodified EG2-X1 (Fig 20a-e). EG2-X6 thrice surpassed the maximal lysis of cetuximab at the highest antibody concentrations (Fig. 20c-e). However, cetuximab consistently achieved maximal specific lysis at considerably lower concentrations than all EG2-hFc hinge-variants, including EG2-X6 (Figs. 18-20).

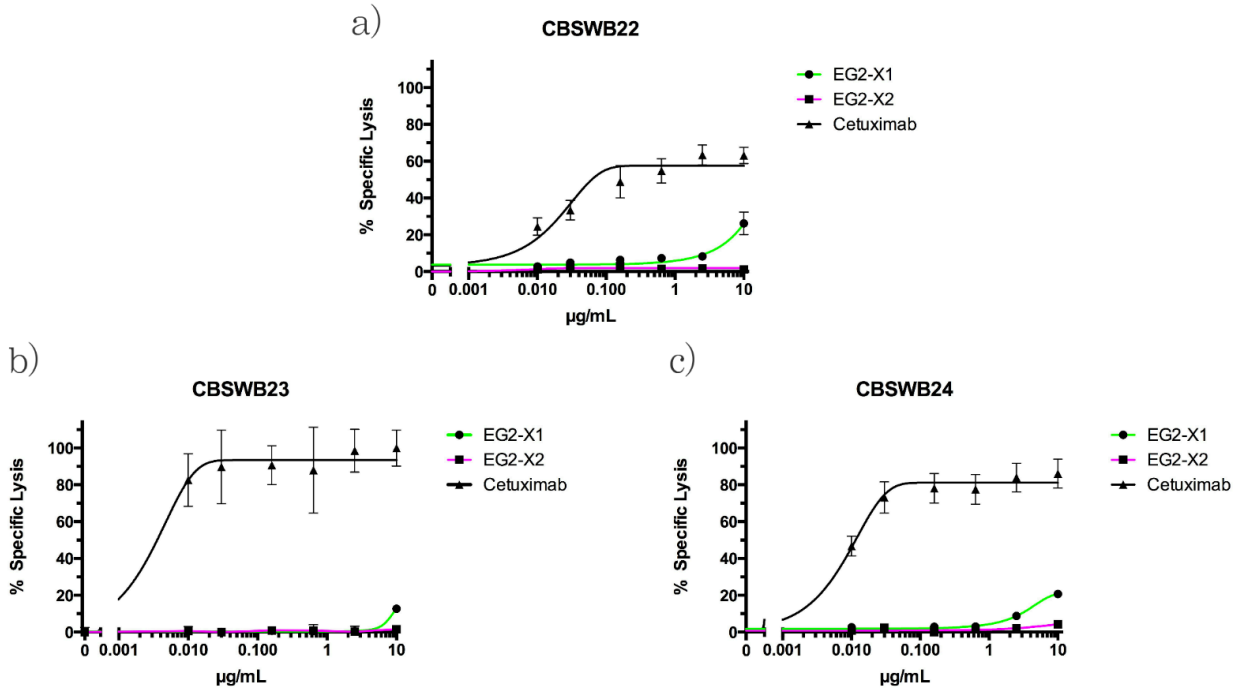

Figure 18: Short-hinge EG2-X2 fails to initiate ADCC

Relative to EG2-X1 and cetuximab, the truncated EG2-X2 repeatedly failed to initiate ADCC across multiple NK cell samples and allotypes at the concentrations tested. Data are presented as mean ± SEM of triplicate wells from individual experiments with the corresponding NK cell donor (CBSWB22-24).

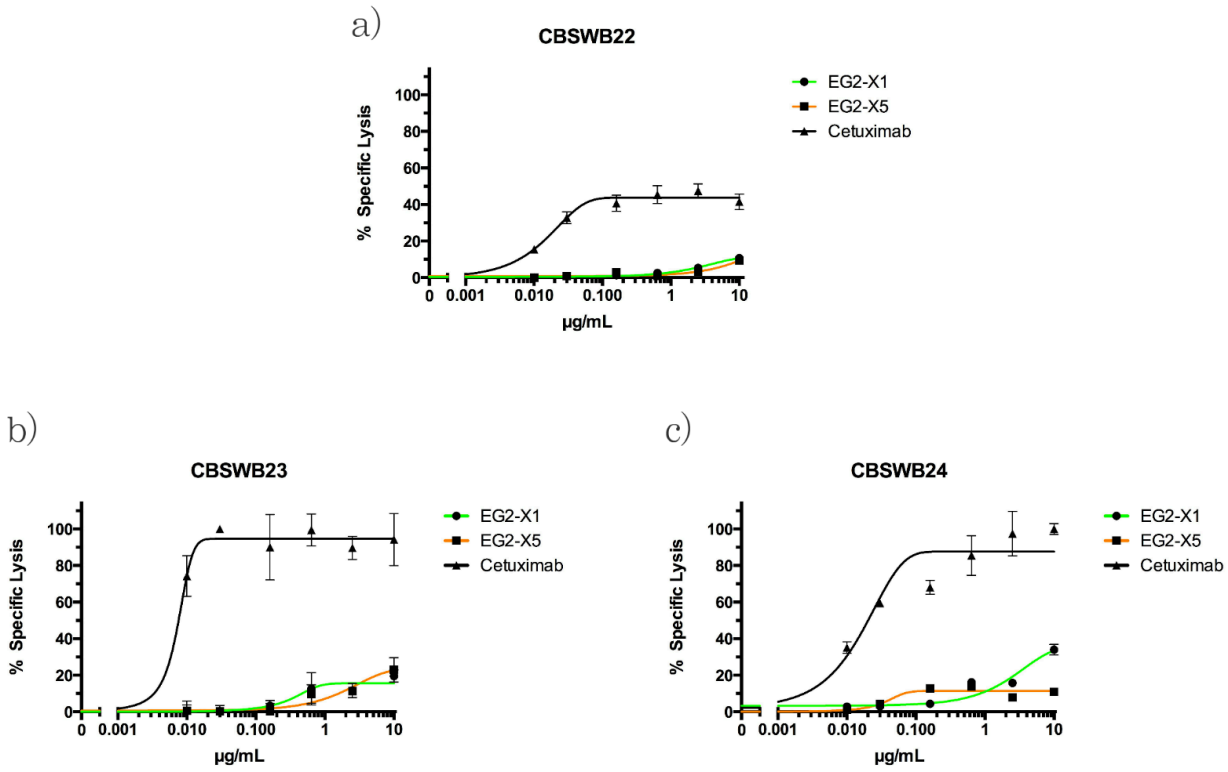

Figure 19: Cysteine-to-serine hinge-variant, EG2-X5, shows ADCC similar to EG2-X1

Though the hinge of EG2-X5 slightly differs from that of EG2-X1, both variants showed largely similar degrees of lysis (a-b). The discrepancy between EG2-X1 and EG2-X5 at the highest concentration did exist with the final NK sample employed (c), which was likely attributable to pipetting errors. Data are presented as mean ± SEM of triplicate wells from individual experiments with the corresponding NK cell donor (CBSWB22-24).

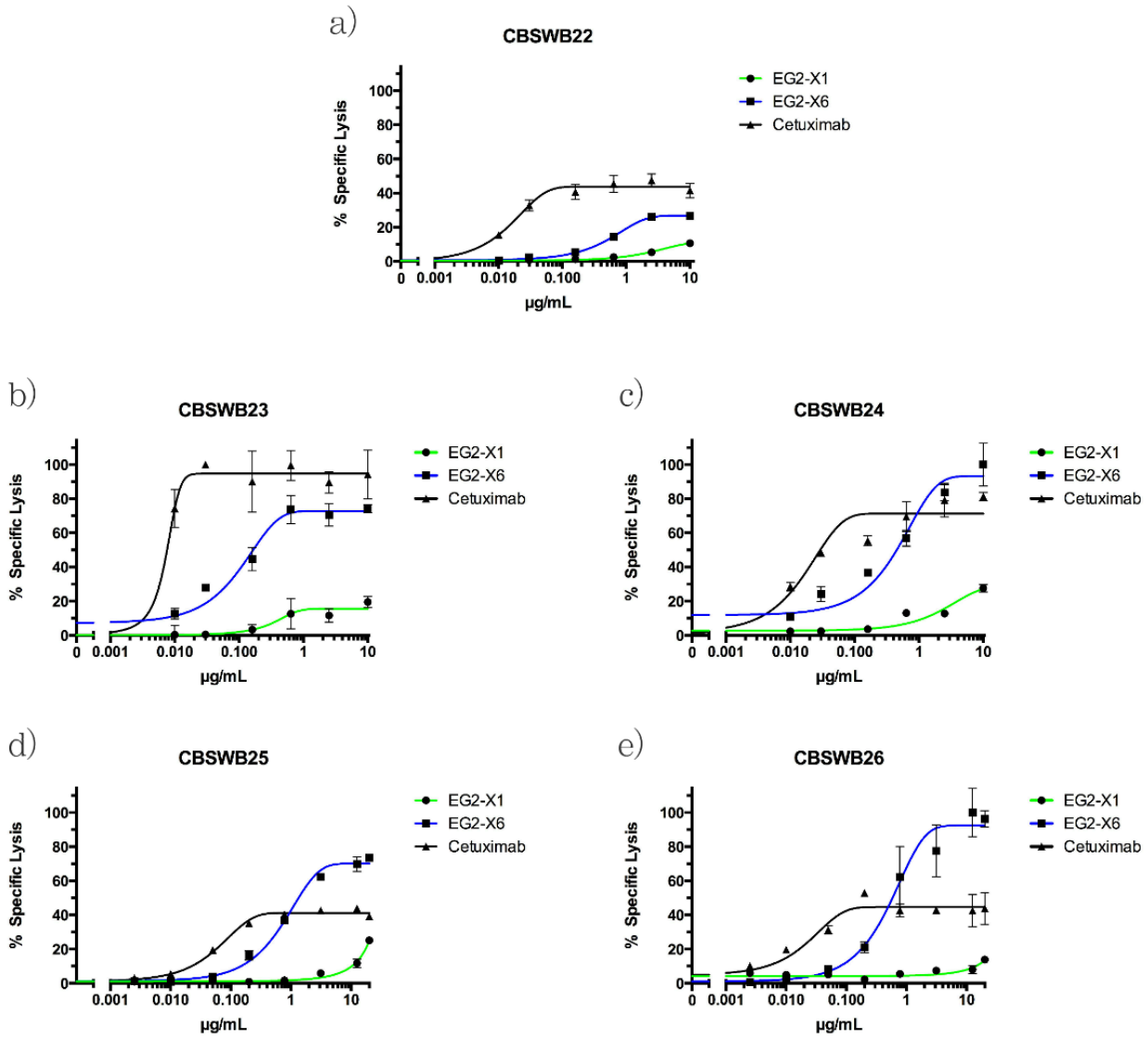

Figure 20: Augmented ADCC by long-hinge EG2-X6

Long-hinge EG2-X6 consistently outperformed EG2-X1, and achieved levels of ADCC comparable to that of cetuximab. Because the lysis achieved by both cetuximab (b) and EG2-X6 (c, e) occasionally surpassed the maximal lysis achieved by 1% cetrimide, these figures were normalized so that 100% of specific lysis corresponded to the highest amount of killing achieved in that particular assay. Data are presented as mean ± SEM of triplicate wells from individual experiments with the corresponding NK cell donor (CBSWB22-26).

4.8 Impact of Asn297 defucosylation on ADCC by EG2-hFc: Following the treatment of CH0-3E7 cells with 5% RMD during expression, the resultant glyco-variant EG2-X7 showed a nearly 25% reduction in Asn297 glycan core-fucosylation compared to unmodified EG2-X1 (data not shown). In agreement with the literature, this decrease in fucosylation corresponded with an overall increase in ADCC: where EG2-X7 consistently exhibited greater lysis than unmodified EG2-X1 (Fig. 21a-e). Similar to what was observed with long-hinge EG2-X6, cetuximab consistently achieved the greatest overall specific lysis at much lower concentrations compared to EG2-X7.

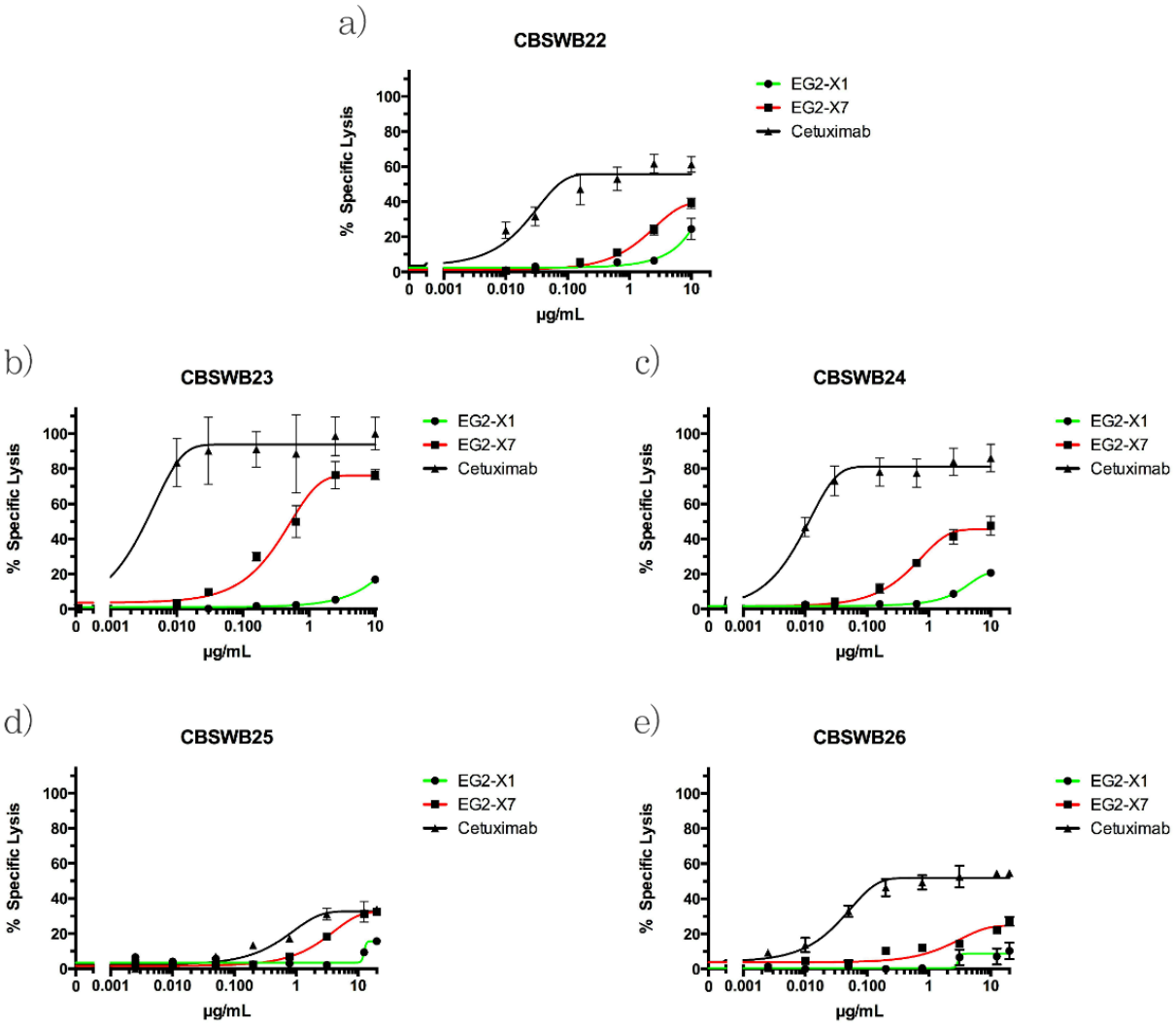

Figure 21: Augmented ADCC by defucosylated EG2-X7

Fc-glycoengineered EG2-X7 consistently outperformed EG2-X1, while achieving levels of ADCC lower than those of cetuximab. Because the lysis achieved by cetuximab (b) occasionally surpassed the maximal lysis achieved by 1% cetrimide, this figure was normalized so that 100% of specific lysis corresponded to the highest amount of killing achieved by cetuximab in the assay. Data are presented as mean ± SEM of triplicate wells from individual experiments with the corresponding NK cell donor (CBSWB22-26).

4.9 Flow-based allotyping of the NK cell V158F CD16a polymorphism: All NK cell samples employed in the CRAs were stained with the FITC-conjugated anti-CD16a mAbs 3G8 and MEM-154, and the resulting MFIs contrasted to ascertain the V158F allotype (Fig. 22). Samples CBSWB13, CBSWB22, CBSWB24 and CBSWB26 all stained negative for the V158-specific mAb, MEM-154: indicating homozygosity for the low-affinity 158FF allotype (Fig. 22). The remaining samples all stained strongly for 3G8 signal, with a slightly less prominent signal from MEM-154: signifying the presence of either the intermediate (158VF) or high affinity (158VV) allotype (Fig. 22). Unfortunately, further differentiation between 158VF or 158VV samples was not possible, leaving the true allotype of these NK cell samples unknown.

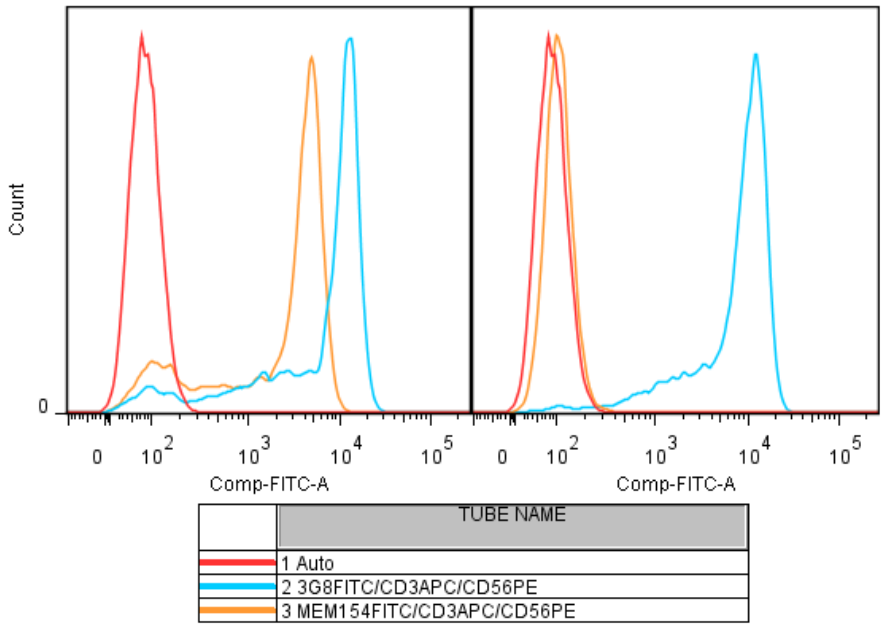

NK cell sample	Predicted V158F allotype
CBSWB8	Intermediate or high affinity (158VF or 158VV)
CBSWB13	Low-affinity 158FF
CBSWB14	Intermediate or high affinity (158VF or 158VV)
CBSWB18	Intermediate or high affinity (158VF or 158VV)
CBSWB21	Intermediate or high affinity (158VF or 158VV)
CBSWB22	Low-affinity 158FF
CBSWB23	Intermediate or high affinity (158VF or 158VV)
CBSWB24	Low-affinity (158FF)
CBSWB25	Intermediate or high affinity (158VF or 158VV)
CBSWB26	Low-affinity (158FF)

Figure 22: Representative CD16a allotyping and list of predicted sample allotypes

a) The left histogram shows strong staining of CBSWB25 NK cells by the 158V-specific mAb MEM-154: indicating either the high-affinity 158VV or intermediate-affinity 158VF CD16a allotypes. Conversely, the right histogram reveals that MEM-154 fails to stain the NK cells of CBSWB26 above background auto-fluorescence, indicating the CD16a receptor to be the low-affinity 158FF allotype. b) The predicted V158F allotype of each sample used.

5. Discussion

5.1 Optimization of the ^{51}Cr release assay

The initial efforts of this investigation focused primarily on ensuring efficiency, accuracy and reproducibility of the CRA through benchmarking of the positive control, cetuximab. FDA approved for the treatment of colorectal, head and neck cancers, cetuximab is a mouse-human chimeric mAb that was initially used for its ability to neutralize oncogenic EGFR. However, a recent investigative push has since revealed cetuximab to be a prodigious mediator of ADCC against EGFR-positive tumours; a therapeutic effect that has begun to overshadow it's intended inhibitory function (9, 16). As a result of the extensive clinical research conducted on cetuximab over the last two decades, it is an ideal positive-control for the optimization and standardization of the variables associated with the ^{51}Cr release assay (CRA): beginning with the selection of an appropriate effector-to-target ratio (E:T) (72). Based on our results, an E:T of 10:1 was selected for its requirement of fewer NK cells while still demonstrating a strong ADCC signal compared to non-specific background lysis. However, attaining even this reduced requirement of NK cells proved challenging, as these cells repeatedly offered poor recoveries and viabilities prior to their experimental use: features indicative of suboptimal sample handling. To remedy this, only fresh NK cells were used for CRAs in order to reduce the cellular stress imposed by repeated freeze-thaw cycles. Additionally, adjustments were made to how the blood products were being harvested and shipped, in order to optimize NK cell recoveries. This included the immediate 1:1 dilution of freshly drawn blood with PBS, followed by the samples shipment and storage at room temperature instead of the more commonly used 4°C. These amendments were motivated by a recently published meta-analysis, which

detailed how the distinct subpopulations of cells that comprise whole blood are differentially impacted by the manner in which the blood sample is drawn, handled and stored (73). The authors stress that in order to specifically maximize NK cell recoveries, unintended granulocyte activation must be kept to a minimum, as this increases granulocyte buoyancy and skews the natural gradient required for effective separation via density centrifugation (73). Once enacted, these modifications improved both the pre- and post-ficoll recoveries of buffy-coat and PBMCs, respectively: leading to an overall increase in NK cell recoveries.

Having developed a reliable means of achieving the required NK cell numbers, focus next shifted towards enhancing the signal to noise ratio by priming the cytotoxic function of the NK cells with the activating cytokine IL-2 (74). As a result of the high cell surface expression of intermediate-affinity IL-2R on NK cells, IL-2 acts as a potent stimulator of NK cell cytotoxicity (74-75). Following their overnight co-culture, IL-2 stimulated NK cells subsequently used in CRAs showed increased ADCC: allowing for a clearer discernment between background and specific lysis. However, it should be noted that overstimulation with IL-2 (>15 hour co-incubation with NK cells) gave a sharp increase in background antibody-*independent* killing, which likely developed from the generation of lymphokine-activated killer (LAK) cells (76). Though these unique cells have gathered interest in regards to their anti-tumour activity, their less discriminate killing contrasts with the more directed and cHCAb-reliant approach employed with ADCC. Consequently, great care was taken to ensure that IL-2 overstimulation was avoided by limiting NK cell exposure to less than 15 hours (76). Finally, in an attempt to use a non-radioactive alternative to the CRA, the calcein-acetyoxymethyl (AM) cytotoxicity assay was also briefly employed. Nearly

identical to the CRA, target cells are instead labeled with non-radioactive calcein-AM, which passively enters the target cell's cytoplasm. Once inside, intracellular esterases hydrolyze calcein AM to give fluorescent calcein, which cannot freely exit the cell (77). Following the addition of effector cells and antibody, if any ADCC has occurred, the amount fluorescence in the supernatant resulting from released calcein, can be correlated with degree of lysis that has occurred; akin to measuring radioactivity following the release of ^{51}Cr (77). Unfortunately, the results gathered from our rudimentary iterations of the calcein-AM cytotoxicity assay indicated it would require extensive and time-consuming optimization. Consequently, the decision was made to exclusively employ the ^{51}Cr release assay, as it readily offered a clear and reliable measure of ADCC.

5.2 Initial characterization of EG2-hFc

Having accounted for these important, though somewhat peripheral variables, focus next shifted to benchmarking the ADCC of cetuximab, as it would be the standard against which all of our EG2-hFc variants would be compared. Strong lysis by cetuximab was achieved at as low as 0.2 μg/mL, and this was selected as the starting concentration for preliminary EG2-hFc comparisons. cHCAb characterization began with EG2-X0; the same variant employed in the preceding 2009 *in-vivo* imaging study (53). Though initial flow-based assays showed binding to EGFR-positive cells, EG2-X0 repeatedly showed lytic responses that were indistinguishable from non-specific background killing: indicating a failure to facilitate ADCC (Fig. 15a-b). Furthermore, when EG2-X0 had its thermo-stability characterized via circular dichroism, an atypical biphasic melting curve was revealed: a feature conspicuously absent from other cHCAbs studied within our group, save for one

other unrelated V_HH-hFc fusion (Fig. 23a). It was subsequently revealed that both EG2-X0 and this unrelated cHCAb derived their Fcs from the same source: suggesting this shared feature may be the basis of this atypical biophysical characteristic. This suspicion was substantiated when the sequence of the Fc in question was compared against the wt Fc of human IgG1, with the former being shown to harbor the following mutations: D270G and Y278H (Fig. 8). To determine whether neither, one, or both of these mutations played a role in the atypical unfolding, two novel Fc fragments were expressed: each containing only one of the two mutations (Fig. 8). Following their analysis, both Fc variants exhibited bi-phasic unfolding, which indicated that both mutations contribute to EG2-X0's thermo-instability (Fig. 23g-h). Furthermore, previous work by Shields et al. specifically revealed that the mutation at D270 results in a loss of ADCC as a result of the Fcs inability to bind CD16a (78). In agreement with this finding, no binding between EG2-X0 and immobilized CD16a was detected by surface plasmon resonance (personal correspondence). Collectively, it appears as though the mutations in the Fc of EG2-X0 likely accounts for the observed lack of ADCC: introducing both structural instability, as well as the inability to effectively interact with the CD16a receptor.

5.3 EG2-hFc affinity/avidity effects and the "binding-site barrier"

To rectify this situation, EG2-X0's mutated Fc was replaced with wt Fc from human IgG1, giving EG2-X1 (Fig. 8). Remarkably, this exchange restored the typical monophasic unfolding, and for the first time permitted ADCC by an EGFR-specific cHCAb (Fig. 15b). However, the maximal lysis achieved by EG2-X1 was significantly lower than that of cetuximab, which likely results from the latters stronger affinity: being ≈ 55 nanomolar

(nM) and ≈ 0.39 nM, respectively (53, 79-80). However, high affinity therapeutics like cetuximab may not necessarily prove optimal when administered *in-vivo*, due to the "binding-site barrier": a phenomenon proposed by Fujimori et al., and elegantly demonstrated by Adams et al. (81-82). In the latter study, researchers compared the bio-distribution of a panel of antibody-based constructs specific for the same antigen, but whose respective affinities varied. Remarkably, *in-vivo* imaging revealed that the mid- to low-affinity variants demonstrated superior tumour penetration and accumulation, while the high affinity constructs were limited to binding exclusively at the tumour's perimeter (82). This phenomenon has been reported elsewhere, and these studies collectively report that tumour-associated antigens expressed at the cell surface, like the EGFR, bind and tie-up high affinity antibodies at the tumours exterior: curtailing their therapeutically favourable migration inwards (81-84). Conversely, lower-affinity binders that fall off of surface antigen more readily may continue moving towards the tumours more interior structures (81). Based on these observations, it is thought that in regards to affinity there exists a threshold of diminishing returns, dictated by the characteristics of both the tumour's structure, as well as the antigen itself. Thus, with the "binding-site barrier" in mind, EG2-X1's relatively intermediary affinity and uniquely small size compared to cetuximab, may synergistically act *in-vivo* to enhance tumour killing via increased tumour penetration and accumulation.

5.4 EG2-hFc hinge modifications

5.4a Impact of hinge shortening and upper-hinge cysteine removal on EG2-hFc ADCC

Though EG2-X1 was able to demonstrate good EGFR binding and ADCC (Figs. 12a, 15b-d), there was uncertainty regarding the status of the vestigial upper-hinge cysteine residues, which in human IgG form an inter-chain DSB with their adjacent V_L; joining the heavy and light chains (85). Given the absence of V_L in cHCAbs, formation of this inter-chain DSB is impossible: introducing ambiguity regarding how these newly available cysteines may be engaged, and whether this impacts EG2-X1 functionality. To resolve this, EG2-X1 had a small portion of its hinge excised, which included the upper-hinge cysteines. The resultant short-hinge variant, EG2-X2, showed only slight reduction in binding to EGFR compared to EG2-X1: indicating the truncation had not greatly impacted its ability to bind antigen (Fig. 12b). However EG2-X2 revealed a T_m consistently lower than EG2-X1, suggesting the removed cysteines may have been contributing to EG2-X1's thermo-stability, perhaps through formation of a novel inter-heavy chain DSB (Fig. 23c). The observed T_m shift (≈ 2°C), though subtle, is not inconsistent with findings from similar investigations studying the role of inter-chain DSB removal in IgG1 (86-87). Furthermore, EG2-X2 repeatedly failed to facilitate ADCC: raising the question of whether the missing cysteine pair or the unusually shortened hinge may have contributed to the loss of cytotoxicity (Fig. 17). To clarify this ambiguity, EG2-X1 had both its upper-hinge cysteines replaced with the structurally analogous amino acid serine, which lacks the thiol group necessary for potential DSB formation. This substitution prevented formation of the potential upper-hinge DSB, while retaining a hinge length similar to wt IgG1, giving EG2-X5 (Fig. 9). Akin to EG2-X2, removal of the upper-hinge cysteines resulted in a slightly lower

T_m: reaffirming that a novel upper-hinge DSB may be contributing to EG2-X1's thermo-stability (Fig. 23d). However, unlike EG2-X2, EG2-X5 demonstrated EGFR binding (Fig. 12c) and ADCC profiles (Figs. 18, 16b) very similar to EG2-X1: implying the hinge shortening, rather than the removal of the upper-hinge cysteines, contributes to EG2-X2's lack of ADCC. This suspicion draws support from earlier studies, which collectively assert that hinge shortening precludes ADCC due to the location of the Fc-CD16a binding site, which is found at the lower hinge-C_H2 junction (60, 64, 88). The authors collectively suggest that by shortening the hinge, the Fab arms, or in this case the V_HH pairs, are brought precariously close to lower-hinge junction: sterically shielding the CD16a binding site and preventing the hFc-CD16a interaction. Furthermore, crystallographic analysis has revealed that IgG1's Fab arms must assume an asymmetrical configuration about the central Fc, in order to expose the CD16a binding site (60). However, the truncated hinge of EG2-X2 likely lacks the segmental flexibility and length required to assume this asymmetric orientation: further obstructing CD16a-Fc binding, leading to a loss of ADCC (60).

5.4b Impact of hinge extension on EG2-hFc ADCC

In response to the effect that hinge truncation had on the CD16a interaction and ADCC, attention was turned to what impact hinge-extension may have on EG2-hFcs ability to facilitate ADCC. Since the distance between the V_HHs in both EG2-X1 and EG2-X2 is uncharacteristically small (80 Å), their configuration likely precludes any avidity effects initiated by simultaneous binding of both V_HHs at once (49, 59). For instance, chelating binding, where both V_HH bind simultaneously to the same EGFR, is unlikely given the improbability that two identical EG2 epitopes reside near enough to allow for co-

engagement by either EG2-X1 or EG2-X2 (59). Furthermore, simultaneous binding to two distinct, dimerized EGFRs would also be unlikely since their mirrored conformation positions their highly immunogenic domain IIIs at opposing outer faces of the complexed receptors (59, 89). As a result of this arrangement, simultaneous binding would likely require a distance between V_HHs more similar to conventional IgG1 (160 Å), which the unusually short hinge-lengths of EG2-X1 and EG2-X2 likely prohibit (49). To explore what would happen if this size restriction were superseded with an antigen binding conformation more akin to conventional IgG1, the hinge of EG2-X1 was replaced with a naturally occurring long-hinge derived from a subpopulation of HCAbs found across camelids (61). The resultant long-hinge variant, EG2-X6, more closely resembles the antigen-binding configuration of a conventional IgG1 (140 Å): with the added distance between the V_HHs likely permitting additional and potentially preferential types of binding (Fig. 9) (49). Remarkably, extending the hinge augmented ADCC, as the long-hinge EG2-X6 consistently showed greater lysis compared to the unmodified EG2-X1 (Fig. 19). At the highest concentrations employed, EG2-X6 even managed to thrice achieve levels of maximal lysis greater than cetuximab (Fig.19c-e). This enhanced killing may be attributable to synergism between EG2-X6's improved avidity and it's smaller size compared to cetuximab, which may impose less competition for space at the cell's surface. This would ultimately result in more EGFR being bound by cHCAbs, and thus a higher proportion of Fcs available to initiate ADCC (90). Furthermore, the camelid derived long-hinge is exceptionally rigid as a result of its proline rich structure, and such rigidity has previously been correlated with dramatically improved CD16a binding and enhanced effector function (63). Though the exact mechanisms behind this improvement is not fully understood, it is

believed that such rigidity may improve the NK cells access to the CD16a binding site at the hinge-Fc interface. (86-87). Conversely, cetuximab's comparatively large size could impose a greater limitation on available space and access to antigen at the cell surface: reducing both the proportion of bound EGFR as well as the resultant lytic response (90). However, though cetuximab's maximal lysis was occasionally surpassed by EG2-X6, it repeatedly achieved maximal specific lysis at much lower concentrations (Fig. 19). This disparity may result from cetuximab's stronger affinity, where available EGFR is bound more readily, and thus saturating binding occurs at lower concentrations. This MOA is reflected by cetuximab's ADCC response, where onsets of both lysis as well as the maximal lytic plateau were both achieved at much lower concentrations compared to EG2-X6 (Fig. 19). Altogether, cetuximab's affinity may account for the saturation and onset of maximal lysis observed at lower concentrations, while at higher concentrations, EG2-X6's smaller size likely permits binding with greater absolute numbers: resulting in its occasionally heightened maximal lysis.

5.5 EG2-hFc and Fc-glycoengineering

5.5a EG2-hFc and CDC

With EG2-X1 having successfully shown an intrinsic capacity for ADCC, we next hoped to ascertain whether modification of the C_H2 glycan would impact the cHCAbs effector function in the same way it does conventional mAbs (34-36, 38-42). Glycoanalysis of EG2-X1 revealed the C_H2 glycoform to predominantly be a complex type heptasaccharide, with high levels of terminal galactose (Fig. 9). Increased galactosylation at the Asn297 glycan has been correlated with augmenting anti-tumour CDC by improving

binding between the C1q component of complement and its C_H2 binding site (37). With this in mind, the CDC of EG2-X1 was investigated through use of a modified CRA, which revealed no intrinsic CDC (Data not shown). In light of recent publications describing the Fc-dependent formation of hexameric IgG1 required for the initiation of CDC, it is unsurprising that the dissimilar structure of a cHCAb would fail to initiate this response (91). As revealed by crystallographic imaging, both Fab arms of human IgG1 adopt a characteristic orientation within the hexamer: with one arm extending outward for antigen binding, while the other aligns itself within the hexameric plane (91). Unlike the much bulkier and elongated Fab arms of human IgG1, the comparatively compact antigen-binding domains (ABDs) of EG2-hFc are likely unable to assume the necessary hexameric orientation, while retaining the ability to monovalently bind antigen (91). Unfortunately, an established anti-EGFR mAb known to facilitate CDC is not readily available, thus preventing the inclusion of a positive control in the CDC ^{51Cr}-release assay (Data not shown). Though no Fc-fusion based constructs have successfully exhibited CDC to date, a more comprehensive investigation into EG2-hFc's complement-dependent response is required.

5.5b Fc-glycoengineering augments ADCC by EG2-hFc

With preliminary results suggesting CDC to be a therapeutic dead-end, our focus returned to ADCC, and whether reducing core-fucosylation at the C_H2 glycan could augment EG2-X1's intrinsic ADCC response. To accomplish this, 5% RMD was introduced to CHO-3E7 cultures in an attempt to express the defucosylated glycovariant, EG2-X7. Following it's successful expression, EG2-X7 showed a marked reduction of Asn297 core fucosylation, from nearly 100% to 75% for EG2-X1 and EG2-X7, respectively. Importantly, this

modification had no discernable impact on either the cHCAbs affinity for the EGFR, or its thermo-stability stability (Figs. 12e, 23f). EG2-X7 did however demonstrate an improved ADCC response compared to EG2-X1 (CHO) (Fig. 20); an improvement likely resulting from the recently defined interaction between the modified hFc glycan, and a similarly *N*-linked glycan found on CD16a (27). Crystallographic studies have demonstrated that this interaction arises following removal of the core fucose from the Asn297 glycan, which increases the distance between the two C_H2 domains (27, 40). This "open" intra-heavy chain conformation allows for a unique carbohydrate-carbohydrate interaction between the Asn260 glycan of the CD16a, and the now unobstructed basal GlcNAc of the C_H2 glycan (27). Though not especially strong, this interaction is believed to enhance Fc-CD16a binding and consequently augment ADCC (27). However, unlike similar studies that have reported over 10-fold increases in ADCC following defucosylation, EG2-X7 exhibits a comparatively smaller increase in effector response relative to EG2-X1 (Fig. 20) (42). This discrepancy likely results from the much lower proportion of defucosylated EG2-X7 compared to the mAbs used in other studies, which often achieve nearly complete afucosylation (41-42). Furthermore, relative to cetuximab, EG2-X6 shows greater overall lysis compared EG2-X7; suggesting that introducing length and rigidity into the cHCAb hinge acts as a better promoter of ADCC than the slightly reduced fucosylation exhibited by EG2-X7 (Fig. 19 v. 20). Though beyond the scope of this investigation, continued reduction of C_H2 fucosylation employed in conjunction with hinge extension, may synergistically act to further augment the antitumour ADCC of EG2-hFc; laying the framework for ways in which to improve the anti-tumor efficacy of cHCAbs.

5.5c ADCC and the CD16a V158F SNP

For each NK sample employed, the respective polymorphism at position 158 was predicted through use of the aforementioned flow-based assay (29). This was performed in an attempt to identify any cHCAb modifications showing reduced allotypic specificity, while accounting for any potential discrepancies observed between CRA results. However, no clear correlations could be drawn between the predicted CD16a allotype and degree of observed lysis, as low-affinity receptors often demonstrated high-overall lysis and vice-versa (Fog. 21). Furthermore, though low-affinity 158FF samples were easily discerned, there was ambiguity in differentiating between intermediate (158VF) and high-affinity (158VV) CD16a samples (Fig. 21). With inconsistency such as this, it is critical to revisit the use of primary effector cells, which when employed in cytotoxicity assays, are notoriously capricious (99). This often gives seemingly inconsistent results, making direct comparison between CRAs inherently challenging (99). Instead, overall trends should be noted, such as how variants behave in relation to one another when characterized with the same NK cell sample, and whether hierarchies of lysis are preserved across multiple NK cell samples. This resolution, though somewhat coarse, provides insight into the relationship between the EG2-hFc constructs and allows for a limited but informed interpretation of the data. It is important to keep these limitations in mind when considering these findings, so as to avoid forming attractive but ultimately unsubstantiated assumptions regarding both EG2-hFc, and cHCAbs in general.

5.6 Future directions:

5.6a EG2-hFc

To further augment EG2-hFc's ADCC, the next logical step would be to subject the cHCAb to both hinge-extension and Fc-glycoengineering simultaneously. Additionally, further increasing the proportion of defucosylated EG2-hFc could similarly augment ADCC, while continuing to abrogate CD16a allotypic-specificity. Eventually, even if the implementation of these combined strategies fail to further augment ADCC, the already impressive *in-vitro* gains observed with both long-hinge EG2-X6 and defucosylated EG2-X7, arguably warrants their further characterization *in-vivo*. Such a transition would permit a clearer and more realistic appraisal of EG2-hFc's therapeutic potential: a perspective that is unavoidably lost *in-vitro*. For instance, the benefit to ADCC resulting from EG2-hFc's ability to accumulate in solid-tumours due to it's small size would be better-resolved *in-vivo*, as the relevant three-dimensional tumour structure and vasculature is not represented *in-vitro*. Historically, discrepancies in therapeutic function between *in-vitro* and *in-vivo* studies have proven essential, as efficacies exhibited in the former context are often disappointingly lost in the latter.

5.6b Multispecific, anti-tumour antibody-based constructs

The modular and amendable nature of both EG2 and V_HHs makes them ideal building blocks for the design of novel multispecific constructs, better able to address the complexities of solid-tumours. The adoption of such strategies has already proven successful in the context of conventional mAbs, with bispecific catumaxomab already approved for the treatment of malignant ascites (98). In addition, numerous other anti-

cancer bispecific mAbs are currently undergoing clinical trials (93). The ability to recognize distinct tumour-associated antigens imparts considerable advantages beyond simply affording a more defined targeting of cancerous cells. For instance, by inhibiting multiple oncogenic signals, bispecific mAbs could potentially avoid the resistance limitations faced by monospecific inhibitory mAbs caused by redundancies in oncogenic signaling (94). In regards to enhancing effector function, a bispecific V_HH-based construct, with one ABD being specific for a TAA and the other being engineered to interact with CD16a, has been proven to be exceptionally promising (95). By using V_HH, researchers were able to enrich for binders that exhibited affinities for the CD16a that far exceeded wt Fc: regardless of the V158F SNP (95). As a consequence, constructs were able to facilitate impressive ADCC, while simultaneously outcompeting endogenous IgG for available CD16a: a limitation that has resulted in the unfeasibly high dosage requirements and production costs of FcR-engaging mAbs (95). Additionally, the investigators propose that dosage requirements could be further mitigated following the addition of a third V_HH specific for FcRn or serum albumin, which would significantly extend the constructs serum retention. By relying exclusively on V_HH, each ABD of such a construct could conceivably be further tailored to possess properties that better permit it to exert its specific function in the unusual tumour microenvironment: akin to the aforementioned *in-vitro* selection of *C. difficile* binders. As part of a construct such as this, EG2 could serve as an effective "warhead," given its proven specificity for both the EGFR and the EGFRvIII. Innovative multispecific binders such as this, along with novel constructs like cHCAbs, have begun to usher in the next generation of antibody-based therapeutics: edging researchers ever closer to the realization of Paul Ehrlich's "magic bullets."

References:

1. Chames, P., Van Regenmortel, M., Weiss, E., Baty, D. 2009. Therapeutic antibodies: successes, limitations and hopes for the future. *British Journal of Pharmacology*. 157: 220-33

2. Kohler, G., Milstein, C. 1975. Continuous cultures if fused cells secreting antibody of predefined specificity. *Nature.* 256: 495-7

3. Glennie, MJ., van den Winkel, JGJ. 2003. Renaissance of cancer therapeutic antibodies. *DDT*. 8(11):503-10.

4. Nicholson, RI., Gee, JM., Harper, ME. 2001. EGFR and cancer prognosis. *Eur. J. Cancer*. 37(4):s9-15.

5. Scott, AM., Wolchok, JD., Old, LJ. 2012. Antibody therapy of cancer. *Nature Reviews Cancer*. 12:278-87.

6. Reichert, JM. (2015, February 6) Therapeutic monoclonal antibodies approved or in review in the European Union or United States. *The Antibody Society*. Retrieved from http://antibodysociety.org/news/approved_mabs.php

7. Beckman, RA., Wiener, LM., Davis, HM. 2007. Antibody constructs in cancer therapy: protein engineering stratagies to improve exposure in solid tumors. *Cancer*. 109:170-9.

8. Ciardiello, F., Tortora, G. 2001. A Novel Approach in the Treatment of Cancer: Targeting the Epidermal Growth Factor Receptor. *Clin. Cancer Res*. 7:2958.

9. Bokenmeyer, C., Van Custem, E., Rougier, P., Ciardiello, F., Heeger, S., Schlichting, M., Celik, I., Kohne, CH. 2012. Addition of cetuximab to chemotherapy as first-line treatment of KRAS wild-type metastatic colorectal cancer: pooled analysis of the CRYSTAL and OPUS randomized clinical trials*. Eur J Cancer*. 48(10):1466-75.

10. Bonner, JA., Harari, PM., Giralt, J., Cohen, RB., Jones, CU., Sur, RK., Raben, D., Baselga, J., Spancer, SA., Zhu, J., Youssaufian, H., Rowinsky, EK., And, KK. 2010. Radiotherapy plus cetuximab for locoregionally advanced head and neck cancer: 5-year survival data from a phase 3 randomised trial, and relation between cetuximab-induced rash and survival. *Lancet Oncol*. 11(1):21-8.

11. Arteaga, CL., Truica, CI. 2004. Challenges in the development of anti-epidermal growth factor receptor therapies in breast cancer. *Semin. Oncol.* 31(S1):3-8.

12. Wheeler, DL., Dunn, EF., Harari, PM. 2010. Understanding resistance to EGFR inhibitors—impact on future treatment strategies. *Nature Reviews Clinical Oncology*. 7:493-507.

13. McDonagh, CF., Huhalov, A., Harms, BD., Adams, S., Paragas, V., Oyama, S., Zhang, B., Luus, L., Overland, R., Nguyen, S., Gu, J., Kohli, N., Wallace, M., Feldhaus, MJ., Kudla, AJ., Schoeberl, B., Nielsen, UB. 2012. Antitumor activity of a novel bispecific antibody that targets the ErbB2/ErbB3 oncogneic unit and inhibits heregulin-induced activation of ErbB3. *Mol Cancer Ther*. 11(3):582-93.

14. Michaelson, JS., Demarest, SJ., Miller, B., Amatuccia, A., Snyder, WB., Xiufeng, W., Huang, F., Phan, S., Gao, S., Doem, A., Farrington, GK., Lugovosky, A., Joseph, I., Bailly, V., Wang, X., Garber, E., Browning, J., Glaser, SM. 2009. Anti-tumor activity of stability-engineered IgG-like bispecific antibodies targeting TRAIL-R2 and LT-beta-R. *MAbs*. 1(2):128-41.

15. Kimura, H., Sakai, K., Arao, T., Shimoyama, T., Tamura, T., Nishio, K. 2007. Antibody-dependent cellular cytotoxicity of cetuximab against tumor cells with wild-type or mutant epidermal growth factor receptor. *Cancer Sci.* 98(8):1275-80.

16. Nakadate, Y., Kodera, Y., Kitamura, Y., Shirasawa, S., Tachibana, T., Tamura, T., Koizumi, F. 2014. KRAS mutation confers resistance to antibody-dependent cellular cytotoxicity of cetuximab against human colorectal cancer cells. *Int. J. Cancer*. 134(9):2146-55.

17. Jutten, B., Dubois, L., Aerts, H., Wouters, BG., Lambin, P., Theys, J., Lammering, G. 2009. Binding of cetuximab to the EGFRvIII deletion mutant and its biological consequences in malignant glioma cells. *Radiother. Oncol*. 92(3):393-8.

18. Iida, M., Brand, TM., Starr, MM., Huppert, EJ., Luther, N., Bahrar, H., Coan, JP., Pearson, HE., Salgia, R., Wheeler, DL. 2014. Overcoming acquired resistance to cetuximab by dual targeting HER family receptors with antibody-based therapy. *Molecular Cancer*. 13:242.

19. Dreier, A., Both, S., Goswami, A., Weis, J. 2012. Cetuximab induces mitochondrial translocalization of EGFRvIII, but not EGFR: involvement of mitochondria in tumor drug resistance? *Tumour Biol*. 33(1):85-94.

20. Wheeler, SE., Suzuki, S., Thomas, SM., Sen, M., Leeman-Neill, RJ., Chiosea, SI., Kuan, CT., Bigner, DD., Gooding, WE., Lai, SY., Grandis, JR. 2010. Epidermal growth factor receptor variant III mediates head and neck cancer cell invasion via STAT3 activation. *Oncogene*. 29(37):5135-45.

21. Trotta, AM., Ottaiano, A., Zannotta, S., Napolitano, M., Nasti, G., Laffaioli, RV., Scala, S. 2013. Fc gamma receptor IIIa polymorphisms correlated with antibody-dependent cell-mediated cytotoxicity (ADCC): anti-EGFR antibodies induced and clinical outcome in metastatic colorectal cancer patients. *Cancer Res*. 73:2393.

22. Fukai L., Nishio, K., Itakura, T., Koizumi, F. 2008. Antitumor activity of cetuximab against malignant glioma cells overexpressing EGFR deletion mutant variant III. *Cancer Sci*. 99(10):2062-9.

23. Iannello, A., Ahmad, A. 2005. Role of antibody-dependent cell-mediated cytotoxicity in the efficacy of therapeutic anti-cancer monoclonal antibodies. *Cancer and Metastasis Reviews*. 24(4):487-99.

24. Voskoboinik, I., Trapani, JA. 2006. Adressing the mysteries of perforin function. *Immunology and Cell Biology*. 84:66-71.

25. Thiery, J., Keefe, D., Boulant, S., Boucrot, E., Walch, M., Martinvalet, D., Goping, IS., Bleackley, RC., Kirchhausen, T., Lieberman, J. 2011. Perforin pores in the endosomal membrane trigger the release of endocytosed granzyme B into the cytosol of target cells. *Nat. Immunol*. 12(8):770-7.

26. Dienstmann, R., De Dosso, S., Felip, E., Tabernero, J. 2012. Drug development to overcome resistance to EGFR inhibitors in lung and colorectal cancer. *Molecular Oncology*. 6(1):15-26.

27. Ferrara, C., Grau, S., Jager, C., Sonderman, P., Brunker, P., Waldhauer, I., Hennig, M., Ruf, A., Rufer, AC., Stihle, M., Umana, P., Benz, J. 2011. Unique carbohydrate-carbohydrate interactions are required for high affinity binding between FcγRIII and antibodies lacking core fucose. *Proc. Natl. Acad. Sci. USA*. 108(31):12669-74.

28. Hatjiharissi, E., Xu, L., Santos, DD., Hunter, Z., Ciccarelli, B., Verselis, S., Modica, M., Cao, Y., Manning, R., Leleu, X., Dimmock, E., Kortsaris, A., Mitsiades, C., Anderson, K., Fox, E., Treon, S. 2007. Increased natural killing expression of CD16, augmented binding and ADCC activity of rituximab among individuals expressing the FcgRIIIa-158 V/V and V/F polymorphism. *Blood*. 110(7):2561-4.

29. Bottcher, S., Ritgen, M., Bruggemann, M., Raff, T., Luschen, S., Humpe, A., Kneba, M., Pott, C. 2005. Flow cytometric assay for determination of FcgammaRIIIA-158 V/F polymorphism*. J Immunol Methods*. 306(1-2):128-36.

30. Lopez-Albaitero, A., Lee, SC., Morgan, S., Grandis, JR., Gooding, WE., Ferrone, S., Ferris, RL. 2009. Role of polymorphic Fc gamma receptor IIIa and EGFR expression level in cetuximab mediated, NK cell dependent in vitro cytotoxicity of head and neck squamous cell carcinoma cells. *Cancer Immunol Immunother*. 58(11):1853-64.

31. Velders, MP., van Rhijn, CM., Oksam, E., Fleuren, GJ., Warnaar, SO., Litvinov, SV. 1998. The impact of antigen density and antibody affinity on antibody-dependent cellular cytotoxicity: relevance for immunotherapy of carcinomas. *Br. J. Cancer*. 78(4):478-83.

32. Tang, Y., Lou, J., Alpaugh, RK., Robinson, MK., Marks, JD., Weiner, LM. 2007. Regulation of Antibody-Dependent Cellular Cytotoxicity by IgG Intrinsic and Apparent Affinity for Target Antigen. *The Journal of Immunology*. 179(5):2815-23.

33. Nodehi, SM., Repp, R., Kellner, C., Brautigman, J., Staudinger, M., Schub, N., Peipp, M., Gramatzki, M., Humpe, A. 2012. Enhanced ADCC Activity of Affinity Maturated and Fc-Engineered Mini-Antibodies Directed against the AML Stem Cell Antigen CD96. *PLoS ONE*. 7(8):e42426.

34. Jeffries, R. 2005. Glycoslyation of Recombinant Antibody Therapeutics. *Biotechnol. Progress*. 21:11-6

35. Stavenhagen, JB. Gorlatov, S., Tuaillon, N., Rankin, CT., Li, H., Burke, S., Huang, L., Johnson, S., Bonvini, E., Koenig, S. 2007. Fc Optimization of Therapeutic Antibodies Enhances Their Ability to Kill Tumor Cells In vitro and Controls Tumor Expansion In vivo via Low-Affinity Activating Fcγ Receptors. *Cancer Res*. 67:8882-90.

36. Repp, R., Kellner, C., Muskulus, A., Staudinger, M., Nodehi, SM., Glorius, P. Akramiene, D., Dechant, M., Fey, GH., van Berkel, PHC., van de Winkel, JGJ., Parren, PWHI., Valerius, T., Gramatzki, M., Peipp, M. 2011. Combined Fc-protein- and Fc-glyco-engineering of ScFv-Fc fusion proteins synergistically enhances CD16a binding but does not further enhance NK-cell mediated ADCC. *Journal of Immunological Methods*. 373:67-78.

37. Kellner, C., Derer, S., Valerius, T., Peipp, M. 2014. Boosting ADCC and CDC activity by Fc engineering and evaluation of antibody effector functions. *Methods*. 65(1):105-113.

38. Jeffries, R. 2009. Glycosylation as a strategy to improve antibody-based therapeutics. *Nature Reviews Drug Discovery*. 8:226-34.

39. Ha, S., Ou, Y., Vlasak, J., Li, Y., Wang, S., Vo, K., Du, Y., Mach, A., Fang, Y., Zhang, N. 2011. Isolation and characterization of IgG1 with asymmetrical Fc glycosylation. *Glycobiology*. 21(8):1087-96.

40. Ferrara, C., Stuart, F., Sondermann, P., Brunker, P., Umana, P. 2005. The Carbohydrate at FcgRIIIa Asn-162: An Element Required for High Affinity Binding to Non-Fucosylated IgG Glycoforms. *Journal of Biological Chemistry*. 281:5032-36.

41. Schlaeth, M., Berger, S., Derer, S., Klausz, K., Lohse, S., Dechant, M., Lazar, GA., Schneider-Merk, T., Peipp, M., Valerius, T. 2010. Fc-engineered EGF-R antibodies mediate improved antibody-dependent cellular cytotoxicity (ADCC) against KRAS-mutated tumor cells. *Cancer Science*. 101:1080-8.

42. Juntilla, TT., Parsons, K., Olsson, C., Lu, Y., Xin, Y., Theriault, J., Crocker, L., Pabonan, O., Baginksi, T., Meng, G., Totpal, K., Kelley, RF., Sliwkowski, MX. 2010. Superior In vivo Efficacy of Afucosylated Trastuzumab in the Treatment of HER2-Amplified Breast Cancer. *Cancer Res*. 70(11):4481-9.

43. Durocher, Y., Butler, M. 2009. Expression systems for therapeutic glycoprotein production. *Current Opinion in Biotechnology*. 20:700-7.

44. Yamane-Ohnuki, N., Kinoshita, S., Inoue-Urakubo, M., Kusunoki, M., Lida, S., Nakano, R., Wakitani, M., Niwa, R., Sakurada, M., Uchida, K., Shitara, K., Satoh, M. 2004. Establishment of FUT8 knockout Chinese hamster ovary cells: an ideal host cell line for producing completely defucosylated antibodies with enhanced antibody-dependent cellular cytotoxicity. *Biotechnol. Bioeng*. 87(5):614-22.

45. Davies, J., Jiang, L., Pan, LZ., LaBarre, MJ., Anderson, D., Reff, M. 2001. Expression of GntIII in a recombinant anti-CD20 CHO production cell line: Expression of antibodies with altered glycoforms leads to an incease in ADCC through higher affinity for FC gamma RIII. *Biotechnol. Bioeng.* 74(4):288-94.

46. von Horsten, HH., Ogorek, C., Blanchard, V., Demmler, C., Giese, C., Winkler, K., Kaup, M., Berger, M., Jordan, I., Sandig, V. 2010. Production of non-fucosylated antibodies by co-expression of heterologous GDP-6-deoxy-D-lyxo-4-hexulose reductase. *Glycobiology*. 20(12):1607-18.

47. Kanda, Y., Yamada, T., Mori, K., Okazaki, A., Inoue, M., Kitajima-Miyama, K., Kuni-Kamochi, R., Nakano, R., Yano, K., Kakita, S., Shitara, K., Satoh, M. 2006. Comparison of biological activity among nonfucosylated therapeutic IgG1 antibodies with three different N-linked oligosaccharides: the high mannose, hybrid, and complex types. *Glycobiology*. 17(1):104-18.

48. Wright, A., Sato, Y., Okada, T., Chang, K., Endo, T., Morrison, S. 200. *In vivo* trafficking and catabolism of IgG1 antibodies with Fc associated carbohydrates of differing structure. *Glycobiology*. 10:1347-55

49. Hamers-Casterman, C., Atarhouch, T., Muyldermans, S., Robinson, G., Hammers, C., Bajyana Songa, E., Bendahman, N., Hammers, R. 1993. Naturally occurring antibodies devoid of light chains*. Nature*. 363:446-448.

50. Muyldermans, S. 2013. Nanobodies: Natural Single-Domain Antibodies. *Annual Review of Biochemistry*. 82:775-797.

51. de Marco, A. 2011. Biotechnological applications of recombinant single-domain antibody fragments. *Microbial Cell Factories*. 10:44

52. Hussack, G., Arbabi-Ghahroudi, M., Mackenzie, CR., Tanha, J. 2012. Isolation and characterization of Clostridium difficile toxin-specific single-domain antibodies. *Methods Mol. Biol*. 911:211-39.

53. Bell, A., Wang, ZJ., Arbabi-Ghahroudi, M., Chang, TA., Durocher, Y., Trojahn, U., Baardnes, J., Jaramillo, ML., Li, S., Baral, TN., O'Connor-McCourt, M., Mackenzie, R., Zhang, J. 2010. Differential tumor-targeting abilities of three single-domain antibody formats. *Cancer Lett*. 289(1):81-90.

54. Kijanka, M., Warnders, FJ., El Khattabi, M., Lub-de Hooge, M., van Dam, GM., Ntziachristos, V., de Vries, L., Oliveira, S., van Bergen EN Henegouwen, PM. Rapid optical imaging of human breast tumour xenografts using anti-HER2 VHHs site-directly conjugated to IRDye 800CW for image-guided surgery. *Eur. J. Nucl. Med. Mol. Imaging*. 40(11):1718-29.

55. Konterman, RE. 2012. Strategies to Extend Plasma Half-Lives of Recombinant Antibodies. *BioDrugs*. 23(2):93-109.

56. Arbabi-Ghahroudi, M., Desmyter, A., Wyns, L., Hamers, R., Muyldermans, S. 1997. Selection and identification of single domain antibody fragments from camel heavy-chain antibodies. *FEBS Lett*. 414(3):521-6.

57. Hussack, G., Mackenzie, CR., Tanha, J. 2012. Characterization of single-domain antibodies with an engineered disulfide bond. *Methods Mol Bio*. 911:417-29

58. Wesolowski, J., Alzogaray, V., Reyelt, J., Unger, M., Juarez, K., Urrutia, M., Cauerhff, A., Danquah, W., Rissiek, B., Scheuplein, F., Schwarz, N., Adriouch, S., Boyer, O., Seman, M., Licea, A., Serreze, DV., Goldbaum, FA., Haag, F., Koch-Nolte, F. Single domain antibodies: promising experimental and therapeutic tools in infection and immunity. Med Microbiol Immunol. 198(3):157-74.

59. Roovers, RC., Vosjan, M., Laeremans, T., el Khoulati, R., de Bruin, R., Ferguson, KM., Verkleji, AJ., van Dongen, G., van Bergen en Henegouwen, P. 2014. A bi-paratopic anti-EGFR nanobody efficiently inhibits solid tumor growth. *Int J Cancer*. 129(8):2013-24.

60. Radvaev, S., Motyka, S., Fridman, WH., Sautes-Fridman, C., Sun, PD. 2001. The Structure of Human Type III Fcg Receptor in Complex with Fc. *The Journal of Biological Chemistry*. 276:16469-77.

61. van der Linden, R., de Geus, B., Stok, W., Bos, W., van Wassenaar, D., Verrips, T., Frenken, L. 2000. Induction of immune response and molecular cloning of the heavy chain antibody repertoire of *Lama glama*. *Journal of Immunoligical Methods*. 240(1):185-95.

62. Maass, DR., Sepulveda, J., Pernthaner, A., Shoemaker, CB. 2007. Alpaca (Lama pacos) as a convenient source of recombinant camelid heavy chain antibodies (VHHs). *J Immunol Methods*. 324(1-2):13-25.

63. Klement, M., Liu, C., Loo, B., Choo, A., Ow, D., Lee, DY. Effect of linker flexibility and length on the functionality of a cytotoxic engineered antibody fragment. *Journal of Biotechnology*. 199:90-97.

64. Dall'Acqua, W., Cook, K., Damschroder, M., Woods, R., Wu, H. 2006. Modulation of the Effector Functions of a Human IgG1 through Engineering of Its Hinge Region. *The Journal of Immunology*. 177(2):1129-38.

65. Yarden, Y. 2001. The EGFR family and its ligands in human cancer: signaling mechanisms and therapeutic opportunities. *Eur. J. Cancer*. 37(4):S3-8.

66. Masuda, H., Zhang, D. Bartholomeusz, C., Doihara, H., Hortobagyi, GN., Ueno, NT. 2012. Role of the epidermal growth factor receptor in breast cancer. *Breast Cancer Res. Treat*. 136(2):331-45.

67. Liang, Z., Zhang, J., Zeng, X., Gao, J., Wu, S., Liu, T. 2010. Relationship between EGFR expression, copy number and mutation in lung adenocarcinomas. *BMC Cancer*. 10:37

68. Gupta, P., Han, SY., Holgado-Madruga, M., Mitra, SS., Li, G., Nitta, RT., Wong, AJ. 2010. Development of an EGFRvIII specific recombinant antibody. *BMC Biotechnology*. 10:72.

69. Banaszczyk, M., Stoczynska-Fidelus, E., Winiecka-Klimek, M., Bienkowski, M., Och, W., Rieske, P., Piaskowski, S. 2013. EGFRvIII—a stable target for anti-EGFRvIII therapy. *Anticancer Res*. 33(12):5343-8.

70. Zhang, J., Liu, X., Bell, A., To, R., Baral, TN., Azizi, A., Li, J., Cass, B., Durocher, Y. 2009. Transient expression and purification of chimeric heavy chain antibodies*. Protein Expression and Purification*. 65(1):77-82.

71. Rogers, LM., Veermani, S., Weiner, GJ. 2014. Complement in Monoclonal Antibody Therapy of Cancer. *Immunol Res*. 59(0):203-10.

72. Cetuximab [Erbitux] will be the gold standard for the treatment of squamous cell carcinoma of the head and beck by 2010. 2007. *PharmacoEconomics & Outcomes News*. 533(1):10.

73. Mallone, R., Mannering, SI., Brooks-Worrell, BM., Durinovic-Bello, I., Cilio, CM., Wong, FS., Schloot, NC. 2011. Isolation and preservation of peripheral blood mononuclear cells for analysis of islet antigen-reactive T cell responses: position statement of the T-Cell Workshop Committee of the Immunology of Diabetes Society. *Clin Exp Immunol*. 1163(1):33-49.

74. Carson, WE., Parihar, R., Lindemann, MJ., Personeni, N., Dierksheide, J., Meropol, NJ., Baselga, J., Caliguiri, MA. 2001. Interleukin-2 enhances the natural killer cell response to Herceptin-coated Her2/neu-positive breast cancer cells. *Eur J Immunol*. 31(10):3016-25.

75. Roda, J., Joshi, T., Butcher, J., McAlees, J., Lehman, A., Tridandapani, S., Carson III, W. 2007. The Activation of Natural Killer Cell Effector Functions by Cetuximab-Coated, Epidermal Growth Factor Receptor-Positive Tumor Cells is Enhanced By Cytokines. *Clin Cancer Res*. 13:6419.

76. Auber, ML., DeHaven, JI., Raich, PC., Rogers, JS., Cromwell, EB., Romero, P., Mahin, EJ., Sosnowski, JT., Lamm, DL. 1991. IL-2/LAK cell treatment for advanced cancers with emphasis on a novel administration. *W V Med J*. 87(8):344-6.

77. Neri, S., Mariani, E., Meneghetti, A., Cattini, L., Facchini, A. 2001. Calcein-Acetyoxymethyl Cytotoxicity Assay: Standarization of a Method Allowing Additional Analyses on Recovered Effector Cells and Supernatants. *Clin Diagn Lab Immunol*. 8(6):1131-5.

78. Shields, R., Namenuk, A., Hong, K., Meng, YG., Rae, J., Briggs, J., Xie, D., Lai, J., Stadlen, A., Li, B., Fox, JA., Presta, LG. 2001. Resolution Mapping of the Binding Site on Human IgG1 for FcgRI, FcgRII, FcgRIII and FcRn and Design of IgG1 Variants With Improved Binding to the FcgR. *The Journal of Biological Chemistry*. 276(9):6591-6604.

79. Kim, EMH., Mueller, K., Gartner, E., Boerner, J. 2013. Dasatinib is synergistic with cetuximab and cisplatin in triple-negative breast cancer cells. *Journal of Surgical Research*. 185(1):231-9.

80. Kim, GP., Grothey, A. 2008. Targeting colorectal cancer with human anti-EGFR monoclonal antibodies: focus on panitumumab. *Biologics*. 2(2):223-8.

81. Fujimori, K., Covell, DG., Fletcher, JF., Weinstein, JN. 1990. A modeling analysis of monoclonal antibody percolation through tumors: a binding-site barrier. *J Nucl Med*. 31:1191-8

82. Adams, G., Schier, R., McCall, AM., Simmons, HH., Horak, EM., Alpaugh, RK., Marks, JD., Weiner, LM. 2001. High affinity Restricts the Localization and Tumor Penetration of Single-Chain Fv Antibody Molecules. *Cancer Res*. 61:4750-5.

83. van Osdol, W., Fujimori, K., Weinstein, JN, 1991. An analysis of monoclonal antibody distribution in microscopic tumor nodules: consequences of a "binding site barrier". *Cancer Res*. 51(18):4776-84.

84. Ovarnstrom, OF., Simonsson, M., Carlsson, J., Tran, TA. Effects of affinity on binding of HER2-targeting Affibody molecules: model experiments in breast cancer spheroids. *Int J Oncol*. 39(2):353-9.

85. Yan, B., Boyd, D., Kaschak, T., Tsukuda, J., Shen, A., Lin, Y., Chung, S., Gupta, P., Kamath, A., Wong, A., Vernes, JM., Meng, GY., Totpal, K., Schaefer, G., Jiang, G., Nogal, B., Emery, C., Vanderlaan, M., Carter, P., Harris, R., Amanullah, A. 2011. Engineering upper hinge improves stability and effector function of a human IgG1. J. Biol. Chem. 287(8):5891-7.

86. Heads, JT., Adams, R., D'Hooghe, LE., Page, MJ., Humphreys, DP., Popplewell, AG., Lawson, AD., Henry, AJ. Relative stabilities of IgG1 and IgG4 Fab domains: influence of the light-heavy interchain disulfide bond architecture. *Protein Sci*. 21(9):1315-22.

87. Wozniak-Knopp, G., Stadlmann, J., Ruker, F. 2012. Stabilization of the Fc fragment of human IgG1 by engineered intradomain disulfide bonds. *PLoS One*. 7(1):e30083.
88. Burton, DR. 1985. Immunoglobulin G: Functional Sites. Molecular Immunology. 22(3):161-206

89. Ogiso, H., Ishitani, R., Nureki, O., Fukai, S., Yamanaka, M., Kim, JH., Saito, K., Sakamoto, A., Inoue, M., Shirouzu, M., Yokoyama, S. 2002. Crystal structure of the complex of human epidermal growth factor and receptor extracellular domains. *Cell*. 110:775-87.

90. Schmidt, MM., Wittrup, KD. 2009. A modeling analysis of the effects of molecular size and binding affinity on tumor targeting. *Mol Cancer Ther*. 8:2861-71.

91. Diebolder, CA., Beurskens, FJ., de Jong, R., Koning, R., Strumane, K., Lindorfer, MA., Voorhorst, M., Ugurlar, D., Rosati, S., Heck, A., van de Winkel, J., Wilson, I., Koster, AJ., Taylor, RP., Ollman Saphire, E., Burton, DR., Schurrman, J., Gros, P., Parren, P. 2014. Complement Is Activated by IgG Hexamers Assembled at the Cell Surface. *Science*. 343(6176):1260-6.

92. Dechant, M., Weisner, W., Berger, S., Peipp, M., Beyer, T., Scheider-Merk, T., Lammerts van Beuren, JJ., Bleeker, WK., Parren, PW., van de Winkel, JG., Valerius, T. 2008. Complement-dependent tumor cell lysis triggered by combinations of epidermal growth factor receptor antibodies. *Cancer Res*. 68:4998-5003.

93. Chames, P., Baty, D. 2009. Bispecific antibodies for cancer therapy: The light at the end of the tunnel? *MAbs*. 1(6):539-47.

94. Castoldi, R., Ecker, V., Wiehle, L., Majety, M., Busl-Schuller, R., Asmussen, M., Nopora, A., Jucknischke, U., Osl, F., Kobold, S., Scheuer, W., Venturi, M., Klein, C., Niederfellner, G., Sustmann, C. 2013. A novel bispecific EGFR/Met antibody blocks tumor-promoting phenotypic effects induced by resistant to EGFR inhibition and has potent antitumor activity. *Oncogene*. 32(50):5593-601

95. Rozan, C., Cornillon, A., Petiard, C., Chartier, M., Behar, G., Boix, C., Kerfelec, B., Robert, B., Pelegrin, A., Chames, P., Teillaud, J., Baty, D. 2013. Single domain antibody-based and linker-free bispecific antibodies targeting FcγRIII induce potent anti-tumor activity without recruiting regulatory T cells. *Mol Cancer Ther*. 12(8):1481-91.

96. Vu, KB., Ghahroudi, MA,m Wyns, L., Muyldermans, S. 1997. Comparison of Llama VH Sequences From Conventional and Heavy Chain Antibodies. Molecular Immunology. 34(16):1121-31.

97. Tan, LK., Shopes, RJ., Oi, VT., Morrison, SL. 1990. Influence of the hinge-region on complement activation, C1q binding, and segmental flexibility in chimeric human immunoglobulins*. Proc. Natl. Acad. Sci*. 87:162-6.

98. Linke, R., Klein, A., Seimetz, D. 2010. Catumaxomab: Clinical development and future directions. *MAbs.* 2(2):129-36.

99. Tada, M., Ishii-Watabe, A., Suzuki, T., Kawasaki, N. 2014. Development of a Cell-Based Assay Measuring the Activation of FcgRIIa for the Characterization of Therapeutic Monoclonal Antibodies. *PLoS ONE.* 9(4): e95787.

100. Bodnar, E., Nascimento, TF., Girard, L., Komatsu, E., Lopez, P., Oliveira, AGG., Roy, R., Symthe, T., Zogbi, Y., Spearman, M., Tayi, VS., Butler, M., Perreault, H. 2015. An Integrated Approach to Analyze EG2-hFc Monoclonal Antibody N-Glycosylation by MALDI-MS. *Canadian Journal of Chemistry*. Doi: 0, 0, 10.1139/cjc-2015-0061.